A simple model of global aerosol indirect effects

Steven J. Ghan,[1] Steven J. Smith,[1] Minghuai Wang,[1] Kai Zhang,[1] Kirsty Pringle,[2] Kenneth Carslaw,[2] Jeffrey Pierce,[3] Susanne Bauer,[4] and Peter Adams[5]

Received 21 February 2013; revised 10 May 2013; accepted 6 June 2013; published 28 June 2013.

[1] Most estimates of the global mean indirect effect of anthropogenic aerosol on the Earth's energy balance are from simulations by global models of the aerosol lifecycle coupled with global models of clouds and the hydrologic cycle. Extremely simple models have been developed for integrated assessment models, but lack the flexibility to distinguish between primary and secondary sources of aerosol. Here a simple but more physically based model expresses the aerosol indirect effect (AIE) using analytic representations of cloud and aerosol distributions and processes. Although the simple model is able to produce estimates of AIEs that are comparable to those from some global aerosol models using the same global mean aerosol properties, the estimates by the simple model are sensitive to preindustrial cloud condensation nuclei concentration, preindustrial accumulation mode radius, width of the accumulation mode, size of primary particles, cloud thickness, primary and secondary anthropogenic emissions, the fraction of the secondary anthropogenic emissions that accumulates on the coarse mode, the fraction of the secondary mass that forms new particles, and the sensitivity of liquid water path to droplet number concentration. Estimates of present-day AIEs as low as -5 W m^{-2} and as high as -0.3 W m^{-2} are obtained for plausible sets of parameter values. Estimates are surprisingly linear in emissions. The estimates depend on parameter values in ways that are consistent with results from detailed global aerosol-climate simulation models, which adds to understanding of the dependence on AIE uncertainty on uncertainty in parameter values.

Citation: Ghan, S. J., S. J. Smith, M. Wang, K. Zhang, K. Pringle, K. Carslaw, J. Pierce, S. Bauer, and P. Adams (2013), A simple model of global aerosol indirect effects, *J. Geophys. Res. Atmos.*, *118*, 6688–6707, doi:10.1002/jgrd.50567.

1. Introduction

[2] The number of aerosol particles in the atmosphere has increased substantially over preindustrial levels due to anthropogenic emissions of aerosol and aerosol precursor gases. A significant fraction of these particles can act as cloud condensation nuclei (CCN), and this increase in number results in clouds with a larger number of water droplets, which makes clouds more reflective of sunlight [*Twomey*, 1977]. Reduction of droplet size can also allow clouds to contain more liquid water before precipitating [*Albrecht*, 1989]. These mechanisms comprise the basis of the aerosol indirect radiative forcing effect.

[3] The indirect effect of anthropogenic aerosol on the Earth's energy balance through the role of particles as CCN is estimated to be large enough to require representation in simulations of past and future climate change [*Penner et al.*, 2001; *Forster et al.*, 2007]. Many of the global climate model (GCM) simulations conducted for the Intergovernmental Panel on Climate Change Fifth Assessment therefore include representations of the aerosol indirect effect (AIE).

[4] However, estimates of the AIE for the preindustrial to present-day period vary widely from model to model, ranging between -0.2 and -2.5 W m^{-2} [*Lohmann et al.*, 2010]. This uncertainty in the AIE is the largest source of uncertainty in estimates of the total radiative forcing of climate change since preindustrial times [*Forster et al.*, 2007; *Storelvmo et al.*, 2009] and poses a considerable impediment to the use of the observed warming as a constraint on the climate sensitivity [*Kiehl*, 2007].

[5] The uncertainty in the AIE is large because it depends on many factors [*Pan et al.*, 1998; *Adams and Seinfeld*, 2003; *Chen and Penner*, 2005; *Haerter et al.*, 2009; *Pierce and Adams*, 2009; *Wang and Penner*, 2009; *Lohmann and Ferrachat*, 2010; *Lee et al.*, 2011, 2013], each of which varies widely in space and time because the lifetime of clouds and aerosol is much shorter (hours to days) than that of most greenhouse gases (years to centuries). These factors include the mass, composition, and size distribution of emitted primary anthropogenic aerosol, the mass of emitted anthropogenic aerosol precursor gas, the fraction of precursor gas that forms secondary aerosol, the fraction of the secondary aerosol that forms

[1]Pacific Northwest National Laboratory, Richland, Washington, USA.
[2]School of Earth and Environment, University of Leeds, Leeds, UK.
[3]Department of Atmospheric Sciences, Colorado State University, Fort Collins, Colorado, USA.
[4]Goddard Institute for Space Studies, New York, New York, USA.
[5]Center for Atmospheric Particle Studies, Carnegie Mellon University, Pittsburgh, Pennsylvania, USA.

Corresponding author: S. J. Ghan, Pacific Northwest National Laboratory, 902 Battelle Blvd., Richland, WA 99352, USA. (steve.ghan@pnnl.gov)

2169-897X/13/10.1002/jgrd.50567

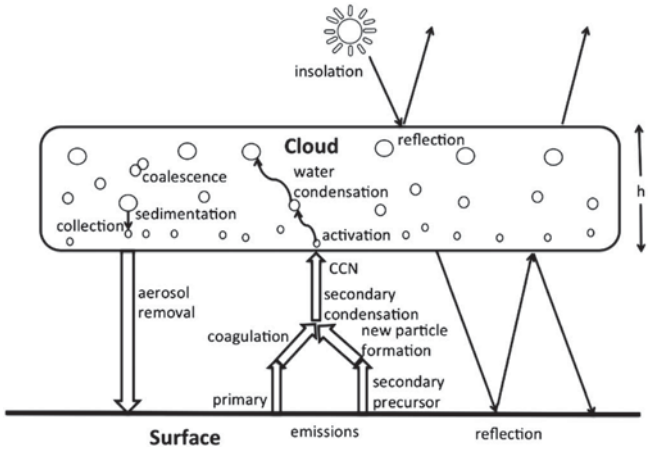

Figure 1. Processes represented in the simple model.

new particles versus condensing to existing particles, the fraction of new particles that survive to grow large enough to serve as CCN, the ratio of aerosol concentration below cloud to the column burden, the fraction of CCN that actually form droplets in clouds (which depends on both updraft velocity and the number of natural as well as anthropogenic CCN), the sensitivity of cloud albedo to changes in droplet number concentration, the sensitivity of cloud liquid water path to droplet number concentration, and the fractional coverage of clouds. In addition, the effects of clouds on aerosol production, subgrid vertical transport, and removal are likely as important as the effects of the aerosol on clouds.

[6] All or most of these factors are included (albeit imperfectly) in the most advanced GCMs that represent the AIE [*Takemura et al*., 2005; *Storelvmo et al*., 2006; *Lohmann et al*., 2007; *Wang and Penner*, 2009; *Donner et al*., 2011; *Wang et al*., 2011; *Bauer and Menon*, 2012; *Ghan et al*., 2012; *Zhang et al*., 2012]. The spatial and temporal variability is explicitly resolved down to scales of hundreds of km horizontally and hours in time. Including this level of detail is computationally expensive, increasing the run time of most GCMs by a factor of at least two. Although efforts are underway to minimize the complexity needed to represent the AIE in GCMs [*Liu et al*., 2012; *Ghan et al*., 2012], any physically based representation must account for all of the above factors, and hence is bound to be quite complex and computationally expensive. Although AIE estimates by GCMs are fraught with uncertainty because they do not resolve clouds and rely on uncertain representations of cloud processes, even global cloud-resolving models, which are several orders of magnitude more expensive than GCMs in most applications, do not resolve all the small-scale processes involved in cloud-aerosol interactions.

[7] In parallel with the representation of the AIE in GCMs, the AIE has also been represented in much simpler models of the global climate system used in integrated assessment models (IAMs) that quickly explore implications of different energy technology decisions. *Kaufman and Fraser* [1991] developed a simple linear model suitable for small perturbations in cloud droplet number concentration. *Wigley and Raper* [1992] used a logarithmic function of global anthropogenic sulfur emissions to represent the AIE in the MAGICC model, which was extended by *Meinshausen et al*. [2011a] to incorporate multiple precursor emissions. The goal of simple climate models such as MAGICC is not to produce first-principle estimates of climate change, but to capture the most relevant effects in a consistent manner in order to quickly produce projections of multiple scenarios.

[8] Although the demonstrated insensitivity of the global mean surface temperature response to the spatial distribution of the radiative forcing [*Hansen et al*., 1997] suggests that the spatial distribution of the forcing is not important, thus justifying the focus on global mean forcing in IPCC assessments and in IAMs, the nonlinear dependence of the AIE on clouds and aerosols indicates that spatial variability in clouds and aerosols should be accounted for even in estimates of the global mean AIE. GCMs do this, but at a considerable computational expense, while IAMs do not.

[9] We develop here an intermediate model of the global mean AIE based on physical principles similar to those used in global atmospheric models and using analytic representations of spatial variations in both clouds and aerosols. Aerosol effects on both droplet effective radius and cloud liquid water path are represented. This model allows rapid exploration of the fundamental assumptions that affect the magnitude of the AIE in a computationally efficient manner. We use this model below to show that the AIE is highly sensitive to poorly constrained variables such as preindustrial aerosol concentrations. We can easily explore the parameter space of the AIE and improve our understanding of the interdependencies of the mechanisms involved. This model could also potentially be used to estimate changes in the AIE within models that include atmospheric chemistry and transport but lack endogenous representations of clouds.

[10] We will use the physically based AIE model developed here, referred below as the "simple model," to examine the sensitivity of the AIE to a range of parameters. We also will test if the simple formulas used in IAMs can capture the range of plausible behavior over the next century as primary and precursor emissions change substantially.

[11] Section 2 describes the model along with the baseline (central case) parameter values. The sensitivity to model parameters is explored in section 3, while section 4 compares GCM estimates with estimates by the model using global mean size distributions from several GCMs. Conclusions are summarized in section 5.

2. Model Description

[12] Figure 1 illustrates the processes represented by the simple AIE model. The following sections describe the treatment of the processes.

2.1. Aerosol Model

[13] The AIE arises because cloud droplets form on aerosol particles that serve as CCN. The simple model developed here begins with the *Abdul-Razzak and Ghan* [2000] parameterization of the number concentration of droplets nucleated, N_d, given a cloud updraft velocity w (a baseline value of 0.3 m s^{-1}), aerosol composition, and multiple log-normal size distributions to be defined in section 2.4. *Ghan et al*.

[2011] show that the *Abdul-Razzak and Ghan* [2000] scheme can be approximated

$$N_d = \sum_m \frac{N_m}{1 + \left(S_m / S_{\max}\right)^{cm}} \quad (1)$$

where N_m is the number concentration of aerosol mode m,

$$S_m = \left(\frac{4A^3}{27\kappa r_m^3}\right)^{1/2}$$

is the supersaturation needed to activate particles with radius equal to the mode radius r_m of the mode, $c_m \equiv 8/\left(3\sqrt{2\pi}\ln\sigma_m\right)$, and the maximum supersaturation in the updraft is diagnosed from the parameterization

$$S_m^2 = 1/\sum_m \frac{1}{S_m^2}\left[f_m\left(\frac{\varsigma}{\eta_m}\right)^{3/2} + g_m\left(\frac{S_m^2}{\eta_m + 3\varsigma}\right)^{3/4}\right] \quad (2)$$

where

$$\eta_m \equiv \frac{2}{\gamma N_m}\left(\frac{\alpha w}{G}\right)^{3/2} \quad (3)$$

$$\varsigma \equiv \frac{2A}{3}\left(\frac{\alpha w}{G}\right)^{1/2}. \quad (4)$$

[14] Here $\alpha = 5.5\times10^{-4}$ m^{-1}, $\gamma = 3.4\times10^{6}$, $G = 8.0\times10^{-9}$ m^2 s^{-1}, and $A = 1.2\times10^{-9}$ m are parameters that depend weakly on temperature and pressure, σ_m is the geometric standard deviation of the size distribution for mode m, and f_m and g_m are simple functions of σ_m [*Abdul-Razzak and Ghan*, 2000]. Aerosol composition affects droplet nucleation through the dependence of S_m on particle hygroscopicity κ [*Petters and Kreidenweis*, 2007], which is determined from volume weighting of the hygroscopicities of the aerosol components, to be described later.

[15] The droplet number estimate is combined with simple cloud and radiation models to estimate the albedo α_c of low clouds, which can be approximated by a simple function of cloud optical depth τ [*Lacis and Hansen*, 1974]:

$$\alpha_c = \frac{\tau}{8 + \tau} \quad (5)$$

where the cloud optical depth is calculated from geometric optics,

$$\tau = \frac{3W}{2\rho_w r_e} \quad (6)$$

where W is the vertically integrated cloud liquid water path, ρ_w is the density of liquid water, and r_e is the droplet effective radius at cloud top (which is where it is most important for scattering sunlight). The effective radius is the droplet surface area-weighted mean particle radius.

[16] The basis of the AIE can be seen in equation (6) where, for a fixed column amount of water in a cloud (W), the cloud optical depth (e.g., reflectivity) increases as the average particle size (r_e) decreases. From equation (5), it is seen that cloud albedo saturates for optical depths much larger than eight. The focus here is on liquid water clouds, since anthropogenic aerosol is much less effective at nucleating ice crystals than cloud droplets [*Lohmann et al*., 2004].

[17] Assuming the cloud is adiabatic, the liquid water content is nearly proportional to the height above cloud base, h. The droplet effective radius can then be expressed from the relationship between number, radius, and volume for spheres, assuming droplet number is uniform with altitude,

$$r_e = \left(\frac{3ah}{4\pi N_d \rho_w}\right)^{1/3}/k \quad (7)$$

where a is the adiabatic liquid water proportionality constant (0.0024 g m^{-4}), and $k = 0.8$ [*Martin et al*., 1994] is the ratio of volume mean radius to effective radius. Although a is known to vary with temperature and pressure, we select a constant value for 15°C and 900 hPa (R. Wood, personal communication, 2013).

2.2. Aerosol Effects on Cloud Water

[18] Equations (6) and (7) account for the cloud brightness effect (also called the first AIE), in which droplet number affects cloud optical depth through changes in effective radius even if cloud liquid water content does not change.

[19] We now consider the cloud water effect, also called the cloud lifetime effect and the second AIE, in which the cloud liquid water content is affected by droplet number through the dependence of autoconversion (droplet collision/coalescence) on droplet number. Given the potential importance of the cloud water effect, we use two different representations of this dependence.

[20] Representation 1 limits the cloud liquid water content when the droplet effective radius exceeds the threshold radius for precipitation formation, r_c. To account for this, we limit r_e to no more than r_c and limit the liquid water content accordingly. If $r_e < r_c$, then the liquid water path for the adiabatic cloud is

$$W = 0.5ah^2 \quad (8)$$

[21] If $r_e > r_c$ we set $r_e = r_c$ and use equation (7) to diagnose the height above cloud base, h_c, where $r_e = r_c$:

$$h_c = \frac{4\pi\rho_w N_d (kr_c)^3}{3a}. \quad (9)$$

[22] The liquid water path becomes

$$W = 0.5ah_c^2 + ah_c(h - h_c). \quad (10)$$

[23] Typical values for r_c are between 8 and 20 μm [*Liu et al*., 2004]. Much larger values turn off the cloud water effect unless the cloud is very thick. The baseline value is chosen to be 12 μm. Results are shown both with ($r_c = 12$ μm) and without ($r_c = 100$ μm) the cloud water effect because under some conditions the cloud water effect may be negligible

[*Ackerman et al*., 2004; *Hill et al*., 2009], or perhaps offset by other effects [*Denman et al*., 2007]. The estimate without this effect is also consistent with the often-used definition of radiative forcing that does not include cloud water effects [e.g., *Forster et al*., 2007]. However, the concept of adjusted radiative forcing, or radiative flux perturbation [*Lohmann et al*., 2010], which accounts for the cloud water response, has been accepted and used by the IPCC for its Fifth Assessment.

[24] The second representation of the cloud water effect is based on the steady-state balances of cloud water, rain, and drizzle number [*Wood et al*., 2009] for a cloud of thickness h:

$$\frac{q_{ad} - q_c}{\tau_{rep}} = A_c + K_c \tag{11}$$

$$A_c + K_c = S_q \tag{12}$$

$$\frac{A_c}{m_{emb}} = S_N \tag{13}$$

where $q_{ad} = ah$ is the adiabatic liquid water content, q_c is the cloud liquid water content after depletion by autoconversion A_c and collection K_c, and τ_{rep} is a cloud water replenishment time scale (1 h baseline value). The autoconversion rate is parameterized in terms of cloud liquid water content and droplet number [*Khairoutdinov and Kogan*, 2000],

$$A_c = 1350\rho(q_c/\rho)^{2.47}N_d^{-1.79}. \tag{14}$$

[25] The collection rate is expressed in terms of q_c and rain water content q_r

$$K_c = \beta q_c q_r \tag{15}$$

where $\beta = 4.7\mathrm{m}^3\mathrm{kg}^{-1}\mathrm{s}^{-1}$. S_q and S_N, the rates of rain and drizzle number removal by sedimentation, are expressed in terms of the bulk terminal velocities of rain water and drizzle number V_q and V_N:

$$S_q = 2q_r V_q/h \tag{16}$$

$$S_N = 2N_d V_N/h. \tag{17}$$

[26] The terminal velocities are expressed in terms of the volume mean radius of rain,

$$r_v = \left[3q_r/\left(4\pi\rho_w N_D\right)\right]^{1/3} \tag{18}$$

using linear parameterizations by *Khairoutdinov and Kogan* [2000]. The drizzle drop embryo mass m_{emb} is specified as that for a 22 micron droplet. Equations (11)–(13) are solved by iteration for the three unknowns q_c, q_r, and drizzle number N_D using equations (14)–(18) and the terminal velocity expressions. Although the treatment of cloud water replenishment is ad hoc, this representation of cloud microphysics is more consistent with the treatment of cloud microphysics in GCMs than is representation 1 and hence is chosen as the baseline treatment. We will explore the dependence of the AIE on the replenishment time scale; from equation (11), it can be seen that if τ_{rep} is very short, the clouds are more adiabatic and the cloud water effect is diminished.

[27] The result of including the cloud water effect is that as aerosol number increases, not only does the effective radius decrease (increasing scattering), but the overall, time-averaged, amount of water in the cloud, or equivalently cloud lifetime, also increases due to lower rates of precipitation formation, which also increases net scattering.

2.3. Distribution of Cloud Properties

[28] Given the sublinear dependence of cloud albedo on optical depth, accounting for variability in clouds is important for correctly representing the sensitivity of the global energy balance to the aerosol. This is done by expressing the variability in the cloud thickness in terms of a normal frequency distribution [*Considine et al*., 1997],

$$\frac{dp(h)}{dh} = \frac{1}{\sigma_h\sqrt{2\pi}}\exp\left[-\frac{(h-h_m)^2}{2\sigma_h^2}\right] \tag{19}$$

where σ_h, the standard deviation of the cloud thickness, can be estimated from satellite retrievals of liquid water path under the adiabatic approximation [*Wood and Taylor*, 2001]. Although *Considine et al*. [1997] estimate σ_h to be 70 m for stratocumulus clouds, such a value only accounts for variability over spatial scales less than $(50\ \mathrm{km})^2$. To account for spatial variability up to global scales, we prescribe the baseline value at 200 m, which is characteristic of the thickness of boundary layer clouds [*Bennartz*, 2007]. The parameter h_m is diagnosed from σ_h and a prescribed value for the low cloud fraction f_c by integrating the cloud thickness distribution (19) over all positive values of h ($h < 0$ is cloud free) and approximating the resulting error function

$$f_c = \frac{1}{2}\left[1 - \mathrm{erf}\left(\frac{h_m}{\sigma_h}\right)\right] \tag{20}$$

using a hyperbolic tangent function [*Ghan et al*., 2011], yielding

$$h_m = -\frac{\sigma_h\sqrt{2\pi}}{4}\ln\left({}^{1}/_{f_c} - 1\right). \tag{21}$$

[29] Integration over the frequency distribution is performed numerically using 20 cloud thickness bins equally spaced between 0 and 3 σ_h. The baseline low cloud fraction is prescribed to be 0.37, the global mean value for low clouds (top pressure > 680 hPa) from Cloud-Aerosol Lidar and Infrared Pathfinder Satellite Observations (CALIPSO) [*Kay et al*., 2012], which with $\sigma_h = 200$ m yields $h_m = -67$ m. Note that h_m is negative for cloud fraction less than 0.5.

2.4. Aerosol Loading and Emissions

[30] Another saturation effect limiting aerosol indirect forcing is the sublinear dependence of droplet number on aerosol number [*Abdul-Razzak and Ghan*, 2000]. To better account for this effect on the global mean AIE and to relate the AIE to aerosol emissions, we express the anthropogenic

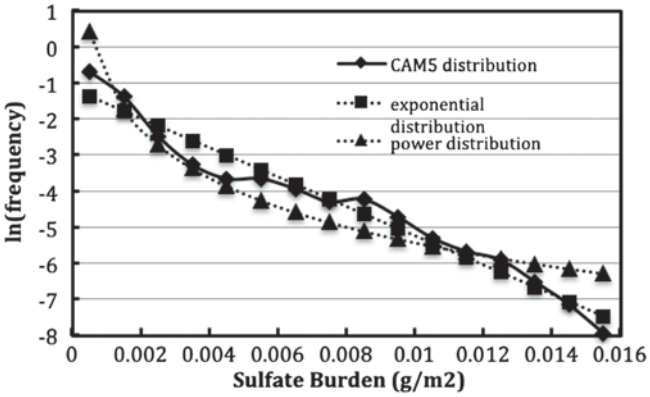

Figure 2. Spatial frequency distribution of annual mean anthropogenic sulfate burden determined from the difference between CAM5 simulations with present-day and preindustrial sulfur emissions, and least square fits with exponential and power law distributions.

aerosol spatial variability in terms of an exponential probability density function (PDF)

$$\frac{dp(M)}{dM} = \frac{1}{M}\exp\left(-\frac{M}{M_m}\right) \tag{22}$$

where M is the anthropogenic aerosol burden, and M_m is the global mean anthropogenic burden, and then relate the aerosol burden to emissions and aerosol number concentration. Support for such a distribution of M is illustrated in Figure 2, which shows the spatial frequency distribution of the annual mean anthropogenic sulfate aerosol burden simulated by the Community Atmosphere Model (CAM5) [*Liu et al*., 2012], along with exponential and power law distribution fits to the simulated distribution. Again, integration over the frequency distribution is performed numerically.

[31] We assume the PDFs for aerosol burden and cloud thickness are uncorrelated. Since deeper clouds are more likely to precipitate and remove aerosol, it is likely that assuming independence is not realistic, but treating such correlations would introduce considerable complexity to the model. Without introducing such complexity, we can only suggest that if cloud depth and aerosol burden are negatively correlated (which is likely given that most aerosol is removed by precipitation from clouds), the estimated AIE would be smaller than estimated here. We will show that for one model, the negative correlation between time mean cloud fraction and aerosol burden reduces the AIE by about 15%. Negative temporal correlations could reduce the AIE further.

[32] The global mean burden of anthropogenic aerosol is estimated from the product of the mass emitted, the fraction that forms aerosol, and the lifetime of aerosol in the atmosphere (chosen to be 4 days based on global simulations of accumulation mode aerosol). We assume the anthropogenic aerosol is a combination of secondary ammonium bisulfate, secondary organic aerosol (SOA), and primary organic matter (POM) and black carbon (BC). We neglect primary emissions of sulfate (aerosol nucleated in the plume of anthropogenic SO_2 sources), which are thought to be smaller in terms of mass than primary emissions of POM [*Stevens et al*., 2012; *Liu et al*., 2012]. Although BC is insoluble and anthropogenic emissions of BC are much less than those of sulfur, it is an important primary source of particle number; POM is emitted with BC. Effects of BC absorption on clouds are not considered.

[33] Since almost all anthropogenic sulfate is derived from SO_2 emissions, the mass emitted is assumed to be SO_2. Since almost all sulfate aerosol is secondary, to account for the ratio of ammonium bisulfate molecular weight to SO_2 molecular weight (1.8) and for the 45% loss of SO_2 by wet and dry deposition before conversion to sulfate [*Liu et al*., 2012], we use an effective emission that is the product of the SO_2 emissions, the fraction of emitted SO_2 that forms sulfate (55%), and the ratio of molecular weights (1.8). The product of 1.8 and 0.55 is 1.0, so the production of ammonium bisulfate is nearly equal to the SO_2 emissions. Although the fraction of SO_2 that forms sulfate is subject to some uncertainty through its dependence on dry and wet deposition, on aqueous chemistry and on oxidant capacity [*Manktelow et al*., 2007], we fold that uncertainty into the emissions and simply consider the forcing as a function of the effective emissions. Present-day (average for years 2000–2005) anthropogenic SO_2 emissions are estimated to be 110 Tg/yr [*Smith et al*., 2011], yielding an effective anthropogenic sulfate source of 110 Tg/yr. Although the natural sulfur emissions are not used in the model because natural aerosol concentrations rather than emissions are prescribed, the effective natural sulfur source that is consistent with the baseline preindustrial surface sulfate concentration simulated by CAM5 and with the assumed aerosol scale height and lifetime is 43 Tg/yr.

[34] Anthropogenic SOA contributes a smaller but not negligible fraction to the total anthropogenic aerosol mass burden. In most global aerosol models, the complexity of organic chemistry is ignored by assuming each volatile organic specie is emitted and instantaneously oxidized to form SOA with a species-specific fractional yield. The effective emissions of anthropogenic SOA is the sum, over all anthropogenic species, of the product of the volatile mass emitted and the yield. For CAM5 [*Liu et al*., 2012], the sum is 14 Tg/yr for year 2000, although this value is quite uncertain.

[35] Recognizing the fact that anthropogenic BC and POM have been emitted since the development of fire as domestic heat source, we limit our baseline estimate of BC and POM emissions to changes since year 1850. Baseline anthropogenic emissions of BC and POM from combustion of fossil fuel, biofuel, and biomass burning over that period are estimated to be 5 Tg/yr and 17 Tg/yr, respectively [*Lamarque et al*., 2010], so the baseline total primary anthropogenic emission is 22 Tg/yr. We use realistic values for the hygroscopicity of ammonium sulfate (0.5), SOA (0.1), BC (0.0), POM (0.0), sea salt (1.2), and dust (0.1) [*Petters and Kreidenweis*, 2007; *Petters et al*., 2009; *Koehler et al*., 2009], and estimate the bulk hygroscopicity of each mode from the volume mean of all components in the mode. Although the hygroscopicity of POM from some sources, such as fires, is order 0.1, the hygroscopicity of POM from fossil fuels, an important anthropogenic source, is much smaller. We also consider cases without primary anthropogenic emissions.

2.5. Aerosol Modes

[36] To relate the aerosol size distribution parameters to the global mean anthropogenic burden, we add the anthropogenic aerosol to a globally uniform natural aerosol. For the

Table 1. Global Mean Surface Values for the CAM5 Aerosol

Mode	Preindustrial	Present Day
	Aitken	
N (# cm^{-3})	155	195
r_n (μm)	0.015	0.016
σ	1.6	1.6
CCN(0.2%) (# cm^{-3})	3.4	5.3
q_{sulf} (μg m^{-3})	0.008	0.013
q_{SOA} (μg m^{-3})	0.001	0.002
$q_{seasalt}$ (μg m^{-3})	0.002	0.002
	Accumulation	
N (# cm^{-3})	250	386
r_n (μm)	0.071	0.067
σ	1.8	1.8
CCN(0.2%) (# cm^{-3})	166	243
q_{sulf} (μg m^{-3})	0.29	0.95
q_{SOA} (μg m^{-3})	0.88	1.06
q_{BC} (μg m^{-3})	0.03	0.09
q_{POM} (μg m^{-3})	0.34	0.56
q_{dust} (μg m^{-3})	1.64	1.64
$q_{seasalt}$ (μg m^{-3})	0.90	0.90
	Coarse	
N (# cm^{-3})	1.70	1.7
r_n (μm)	0.784	0.784
σ	1.8	1.8
CCN(0.2%) (# cm^{-3})	1.7	1.7
q_{sulf} (μg m^{-3})	0.009	0.022
q_{dust} (μg m^{-3})	26.0	26.0
$q_{seasalt}$ (μg m^{-3})	13.7	13.7
Total CCN(0.2%) (# cm^{-3})	171	250

natural aerosol, we use the global and annual mean number and mass concentrations in the lowest layer of global aerosol model simulations with emissions for preindustrial conditions. Table 1 lists the values of the number concentration N_n, number mode radius r_n, and geometric standard deviation σ for each lognormal mode for preindustrial (natural) and present-day CAM5 simulations [*Liu et al*., 2012; *Ghan et al*., 2012]. The preindustrial CAM5 values are selected for baseline estimates. Assuming a uniform distribution of preindustrial aerosol is questionable, as the annual mean CCN concentration simulated by CAM5 for year 1850 varies by more than an order of magnitude, but accounting for such diversity would introduce much more complexity into the model.

[37] The baseline model divides aerosols into three modes based on size: Aitken mode (10–50 nm), accumulation mode (50 - 500 nm), and coarse particles (0.5 –10 μm). To add the anthropogenic aerosol to the natural aerosol, we must decide how to distribute the anthropogenic aerosol across the modes and how much of the secondary anthropogenic aerosol goes into forming new particles rather than just adding mass to existing particles (primary or secondary). Several options were considered for distributing the anthropogenic aerosol across the modes. If all secondary anthropogenic aerosol arises from condensation of precursor gases, then the anthropogenic aerosol is diffusion limited and should be distributed according to the surface area of the modes. But models of the sulfur lifecycle in the atmosphere [*Koch et al*., 1999; *Chin et al*., 2000; *Liu et al*., 2012] indicate that most sulfate is produced by aqueous chemistry in cloud droplets, not by condensation. If all cloud droplets are the same size and aqueous production is proportional to droplet volume then the same amount of sulfate is produced on each activated particle, so aqueous production should be distributed according to the number of particles activated.

[38] For simplicity, one might therefore assume anthropogenic mass is distributed across modes in proportion to the preindustrial CCN concentration in each mode. Although CCN concentration generally depends on supersaturation, which varies with updraft velocity and aerosol concentration, we estimate the CCN concentration from equation (1) for a fixed supersaturation of $S = 0.2\%$ because accounting for the dependence of supersaturation on updraft velocity and aerosol concentration would require iterations as the aerosol concentration would depend on the CCN concentration. These CCN concentrations are only used for the distribution of anthropogenic mass across modes, which is uncertain because it involves multiple processes (condensation and aqueous production) with very different size and number dependencies. Yet as we will show, this method works well in reproducing the aerosol distribution in more complex models in most cases. Values of the CCN concentration at $S = 0.2\%$ for each mode are listed in Table 1. The preindustrial CCN concentration in CAM5 is dominated by the contribution from the accumulation mode; in section 4, we show that this is true for most global aerosol models. In section 3, we shall show that this baseline treatment yields estimates of aerosol indirect forcing smaller (larger) than estimates based on a treatment that distributes anthropogenic mass in proportion to aerosol number (surface area) of the modes. For the primary anthropogenic aerosol (BC and POM), we assume all of it is emitted in the accumulation mode with a mode radius of 0.05 μm and explore the dependence of the AIE on the value of the primary mode radius.

[39] The fraction f_{new} of the secondary anthropogenic aerosol mass that produces new aerosol particles in a mode depends on formation of new particles in the atmosphere, which is poorly understood [*Reddington et al*., 2011]. In this simple model, we either prescribe f_{new} for each mode or diagnose its value based on values from global aerosol models. Assuming that new particles formed only from secondary anthropogenic material, particles composed of natural and secondary anthropogenic material, and particles composed of primary and secondary anthropogenic material all have the same size distribution, the aerosol number balance can be written

$$N_{PD} = N_{nat} + N_{prim} + f_{new} q_{\mathrm{sec}} \frac{N_{PD}}{q_{PD}} \tag{23}$$

where N_{nat}, N_{prim}, and N_{PD}, are, respectively, the natural (preindustrial), primary anthropogenic, and present-day (natural + anthropogenic) number concentration, q_{sec} is the secondary anthropogenic aerosol mass concentration, and $q_{PD} = q_{nat} + q_{prim} + q_{sec}$ is the present-day mass concentration (all concentrations in the model are given by the aerosol burden divided by the scale height of the aerosol—which is estimated to be 3 km from the ratio of the global mean column burden of accumulation mode sulfate aerosol to the surface concentration simulated by CAM5). Note that with this assumption, f_{new} should be interpreted as the fraction of secondary material that produces particles of the size of the mode radius, so it accounts for growth from molecular

clusters to the size of the mode. Since the growth involves coagulation (which destroys number) as well as condensation (which does not), it is difficult to relate f_{new} to the new particle formation rate.

[40] If f_{new} is prescribed, then equation (23) is used to diagnose N_{PD}, and the present-day mode radius is diagnosed from the ratio of q_{PD} to N_{PD}. This permits applications of the simple model to various emission scenarios in which q_{PD} is diagnosed from prescribed emissions.

[41] If instead f_{new} is diagnosed from global aerosol models, then N_{nat}, N_{prim}, N_{PD}, q_{sec}, and q_{PD} in equation (23) are taken from preindustrial and present-day global mean concentrations simulated for each mode by the global aerosol models. The secondary anthropogenic concentration is assumed to be sulfate and SOA. The primary anthropogenic number concentration is estimated from the anthropogenic (present day minus preindustrial) BC and POM mass concentration q_p and an assumed log-normal size distribution:

$$N_{prim} = \frac{3q_{prim}}{4\pi\rho_a r_{prim}^3}\exp\left(-\frac{9\ln^2\sigma_{prim}}{2}\right) \tag{24}$$

where r_{prim} and $\sigma_{\mathrm{prim}} = 1.8$ are the number mode radius and geometric standard deviation of the primary particle size distribution. Under the unrealistic assumption that coagulation of primary emissions can be neglected, r_{prim} is the same as the emitted radius, 0.04 μm [*Liu et al.*, 2012], which, for the anthropogenic primary aerosol mass concentration simulated by CAM5 (0.28 μg m^{-3}) and an aerosol material density ρ_a of 1.77 g cm^{-3}, yields $N_{prim} = 125$ cm^{-3}, which is slightly less than the simulated anthropogenic change in accumulation mode aerosol number concentration, 136 cm^{-3}. The value of f_{new} for the accumulation mode diagnosed from the aerosol number balance equation (23) would be 0.17. If, instead, coagulation is assumed to cause all of the increase in the number mode radius to that of the accumulation mode (0.071 μm), we find that $N_{prim} = 23$ cm^{-3} and from equation (23) with parameter values from Table 1 we find f_{new} is slightly larger than 1. The effective value of the primary number mode radius is somewhere between the emitted radius and the global mean radius of the accumulation mode, because much of the increase in the size of the accumulation mode beyond the emitted size is due to condensation.

[42] The value of f_{new} that is consistent with the number concentration and mass concentrations of primary and secondary aerosol simulated by CAM5 for present-day and preindustrial emissions can be used to constrain the assumed radius of the primary particles, but not the value of f_{new}. If we assume $f_{new} = 0$, then the number of anthropogenic primary particles must equal the anthropogenic increase in the number of accumulation mode particles, which according to Table 1 is 136 cm^{-3} for CAM5. For the 0.28 μg m^{-3} anthropogenic increase in global mean BC and POM surface concentration and the 1.8 geometric standard deviation for the accumulation mode, such an anthropogenic increase in primary particle number implies, using equation (24), $r_{prim} = 0.038$ μm, which is slightly smaller than the emitted size. If instead we assume $f_{new} = 1$, then the number of anthropogenic primary particles diagnosed from equation (23) and the CAM5 parameter values is 32 cm^{-3}, which for the anthropogenic primary mass concentration implies $r_{prim} = 0.078$ μm, which is slightly larger than the accumulation mode radius (0.071 μm). Thus, the information available from CAM5 is consistent with values of f_{new} between 0 and 1 and r_{prim} between 0.04 and 0.71 μm, which are perhaps not coincidentally the emitted and average size of the primary particles, respectively. Thus, although equation (23) can be used to ensure consistency between f_{new} and r_{prim}, it provides little constraint beyond what values of each are physically plausible. We will therefore assume the baseline r_{prim} =0.05 μm but examine the sensitivity of the AIE to r_{prim} over the range 0.04 to 0.07 μm, and assume a baseline value for f_{new} of 0.5 and explore the sensitivity of the AIE to the values of f_{new} between 0 and 1. The aerosol number balance can only be used to enforce consistency between f_{new} and r_{prim} if N_{PD} is known, such as from a global aerosol model. If present-day or future aerosol concentrations are estimated from emissions, then N_{PD} must be estimated from equation (23); then f_{new} and r_{prim} can be prescribed independently.

[43] It might seem that distributing secondary anthropogenic aerosol mass in proportion to CCN concentration is physically inconsistent with designating a certain fraction of the secondary anthropogenic aerosol to form new particles, as new particles are too small to activate as CCN and accumulate secondary anthropogenic aerosol through aqueous chemistry. However, new particles can grow through coagulation and condensation to reach CCN size. Thus, the parameter f_{new} should not be regarded as the fraction of secondary anthropogenic aerosol that makes new particles, but the fraction that makes new CCN. This is consistent with the assumption that all particles in a mode have the same size distribution, regardless of how much of their composition is natural, primary anthropogenic, or secondary.

2.6. Global Energy Balance

[44] Finally, the AIE is determined from the difference between the solar energy balance E with and without anthropogenic emissions. In each case, the solar energy balance for a two-stream radiative transfer model can be written [*Donohoe and Battisti*, 2011], accounting for multiple reflections between the cloud and surface, as

$$E = 0.25S_0\left[(1-f_c)(1-\alpha_s) + \frac{f_c(1-\alpha_c)(1-\alpha_s)}{1-\alpha_c\alpha_s}\right] \tag{25}$$

where S_0 is the downward solar at the top of the atmosphere (1367 W m^{-2}), the factor 0.25 accounts for the ratio of the planet cross section to surface area, the surface albedo α_s is approximated by a single baseline value (0.1). The global mean energy balance is determined by numerical integration over the frequency distributions of the anthropogenic aerosol burden and the cloud thickness, using 10 aerosol bins of equal area and 20 cloud thickness bins of equal cloud thickness interval. For the baseline parameters, the global mean planetary albedo $\alpha_p = 1 - E/S_0$ is 0.20, which is much less than the observed albedo of the Earth, 0.30, because the simple model only accounts for the influence of shallow liquid clouds on the global energy balance. The global mean liquid water path of the shallow clouds is 180 g m^{-2}.

Table 2. Minimum, Baseline, and Maximum Value of Model Parameters

Parameter	Minimum	Baseline	Maximum
Preindustrial accumulation mode N (cm^{-3})	70	250	300
Preindustrial accumulation mode radius (μm)	0.05	0.071	0.10
Accumulation mode σ	1.6	1.8	2.0
Cloud thickness σ_h (m)	70	200	500
Updraft velocity (m s^{-1})	0.1	0.3	1.0
Cloud water replenishment time scale τ_{rep} (s)	600	3600	14,400
Threshold radius for autoconversion r_c (μm)	10	12	20
Anthropogenic BC + POM emissions (Tg/yr)	11	22	44
Anthropogenic SO_2 emissions (Tg/yr)	81	110	150
Anthropogenic SOA emissions (Tg/yr)	7	14	100
Primary mode radius r_{prim} (μm)	0.03	0.05	0.07
Mass fraction new particles f_{new}	0.2	0.5	0.8
Low cloud fraction f_c	0.25	0.37	0.40
Fraction of secondary aerosol mass on accumulation mode	0.8	97	1

3. Sensitivity to Model Parameters

[45] The AIE depends on the uncertain values of several key parameters. Here we explore the dependence on anthropogenic emissions of primary particles (BC + POM) and secondary aerosol precursor gases (SO_2), the partitioning of the secondary emissions across the aerosol modes and between mass and number within each mode, on the threshold radius for precipitation formation, on the parameters of the natural and primary anthropogenic size distributions, and on cloud thickness and updraft velocity. The baseline consists of the three CAM5 aerosol modes, with preindustrial aerosol parameters for CAM5 listed in Table 1. Other baseline parameters and the range of values considered in sensitivity tests are listed in Table 2.

[46] The ranges are limited to the range of plausible values for each parameter. The range in preindustrial accumulation mode number concentration is taken from the global mean simulated by the various aerosol models described in section 4. The range in accumulation mode radius is taken from the same models. The range in accumulation mode σ spans the range in values prescribed in aerosol models plus higher values supported by observations [*Whitby*, 1978]. The lower limit in cloud thickness standard deviation is from *Considine et al*. [1997], while the upper limit is from *Bennartz* [2007]. The range in updraft velocity spans the range observed in boundary layer clouds, while the range in threshold radius for autoconversion is from *Liu et al*. [2004]. The cloud water replenishment time scale is poorly constrained, so a wide range in values is used. Although SO_2 emissions are known to within 10% [*Smith et al*., 2011], we consider a wider range (36% uncertainty) to account for 24% uncertainty in the conversion to sulfate and 27% uncertainty in the sulfate lifetime [*Schulz et al*., 2006]. BC and POM uncertainty emissions uncertainty is assumed to be a factor of 2 [*Bond et al*., 2007]. For anthropogenic SOA, we assume a factor of 2 for the lower bound, but base a much higher upper bound on recent syntheses of measurements and modeling [*Hallquist et al*., 2009; *Spracklen et al*., 2011; *Jathar et al*., 2011]. The radius of primary particles spans the size of primary emissions from different models [*Zhang et al*., 2012] to the size of accumulation mode particles. Low cloud fraction ranges from the ISCCP satellite estimate [*Rossow and Schiffer*, 1999] to 0.4 simulated by some climate models. The fraction of secondary mass on the accumulation mode ranges from 0.8 for the United Kingdom Chemistry and Aerosol (UKCA) model [*Mann et al*., 2010] to nearly 1 for CAM.

[47] Before exploring the parameter space, we first determine the importance of accounting for the spatial variability in the anthropogenic aerosol. Figure 3 shows, for the baseline parameter values, the estimated baseline AIE and the anthropogenic burden for each of the 10 equal-area burden bins in the numerical integration over the exponential PDF of anthropogenic aerosol burden. As expected from the sublinear dependence of droplet number on aerosol number and the sublinear dependence of cloud albedo on cloud optical depth, the estimates of AIE for each bin increase sublinearly with anthropogenic burden. Because of this nonlinearity, representing the spatial variability in the anthropogenic burden is important; the global mean AIE estimated with and without this spatial variability is -1.17 W m^{-2} and -1.32 W m^{-2}, respectively. This sensitivity does not account for the dependence on the location of the burden, particularly with respect to incoming solar radiation.

[48] Figure 4 shows how the AIE depends on primary anthropogenic emissions and on the fraction of secondary anthropogenic material that forms new particles. If primary emissions are neglected, the forcing increases nearly linearly with the fraction after an offset of -0.47 W m^{-2} when the fraction is zero, i.e., when all of the secondary anthropogenic aerosol increases the size of preexisting aerosol particles, so that slightly more particles are activated at a given supersaturation. The forcing is more than twice as strong when all of the secondary anthropogenic mass produces new particles. Adding primary emissions also produces much stronger forcing, by 0.4 W m^{-2}, with a much larger relative influence when $f_{new} = 0$ than when $f_{new} = 1$.

[49] Although according to Figure 4, the primary anthropogenic aerosol significantly increases the AIE, as shown in Figure 5, the impact depends on the assumed mode radius of the emitted aerosol, which determines the number concentration. We have chosen our baseline mode radius for emitted aerosols to be 0.05 μm. Near sources, the emitted particles are near their emitted radius (0.04 μm) but coagulate rapidly,

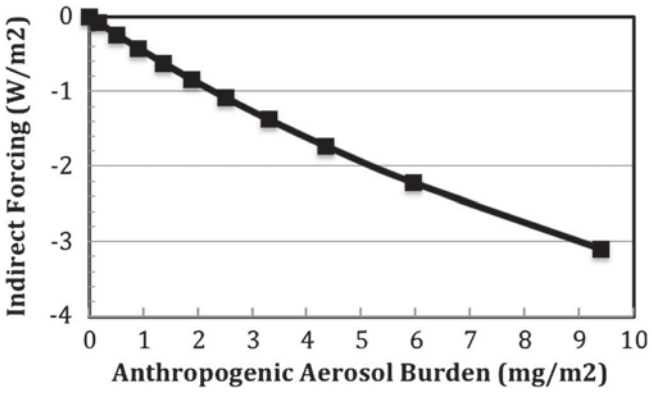

Figure 3. Indirect forcing and anthropogenic aerosol burden in each of the 10 burden bins for the baseline case.

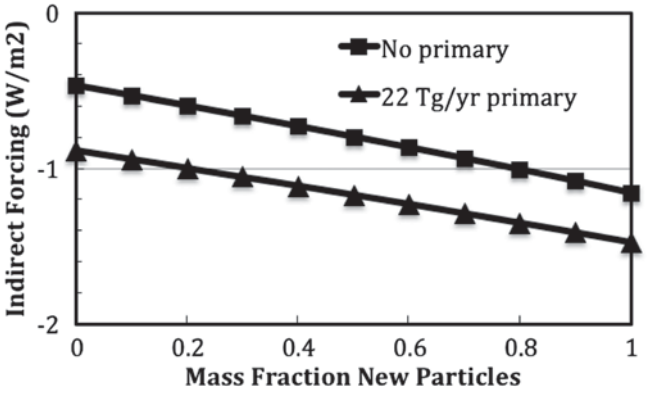

Figure 4. Indirect forcing as a function of mass fraction of baseline secondary anthropogenic emissions making new particles (f_{new}), with and without 22 Tg/yr primary emissions, for the secondary anthropogenic aerosol added to the CAM5 modes in proportion to the CCN concentrations of the modes for the CAM5 preindustrial aerosol.

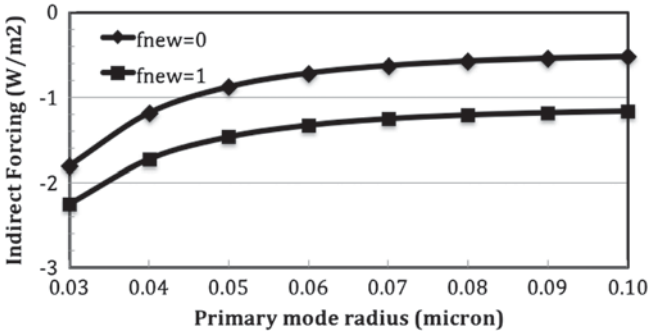

Figure 5. Indirect forcing as a function of the mode radius of the 22 Tg/yr primary anthropogenic aerosol, for baseline secondary anthropogenic emissions added to the CAM5 modes in proportion to the CCN concentrations of the modes for the CAM5 preindustrial aerosol, for $f_{new} = 0$ and $f_{new} = 1$.

increasing their size and decreasing their number concentration. Although we do not expect coagulation alone to lead to a mode radius as large as the accumulation mode radius (0.071 μm) because that includes effects of secondary aerosol production as well coagulation, the most appropriate primary emissions mode radius to assume in the simple model, which does attempt to simulate the effects of coagulation explicitly, should be somewhere between the radius emitted in the global aerosol model and the radius of the accumulation mode. According to Figure 5, the assumed emitted radius between these values can influence the AIE by a factor of 1.9 for $f_{new} = 0$ and 1.4 for $f_{new} = 1$. Although the sensitivity of AIE to emitted size is significant for that size range, it is noteworthy that the combinations of f_{new} and r_{prim} that are both consistent with the anthropogenic changes in the aerosol simulated by CAM5, such as $f_{new} = 0$ for $r_{prim} = 0.04$ and $r_{prim} = 0.078$ for $f_{new} = 1$, yield similar estimates of AIE (-1.19 and -1.22 W m^{-2}).

[50] To explore the dependence of the AIE on the distribution of the secondary anthropogenic mass across the modes, Figure 6 shows the indirect forcing as a function of the fraction of secondary anthropogenic mass distributed to the accumulation mode of the CAM5 aerosol, for two cases: the remaining mass added to (a) the coarse mode, and (b) the Aitken mode. In both cases, the forcing is stronger as a larger proportion of the secondary anthropogenic mass is distributed to the smaller mode, increasing the anthropogenic contribution to aerosol number concentration. The forcing tends to saturate as the proportion on the Aitken mode approaches one, because some of the Aitken particles are too small to form cloud droplets and cannot compete with the primary particles.

[51] The aerosol effect on cloud water is represented in climate models through the treatment of autoconversion. Some climate models use the *Khairoutdinov and Kogan* [2000] autoconversion scheme adopted in Representation 2. Others express autoconversion in terms of the threshold radius, r_c, for precipitation formation, which is used in Representation 1. To explore the dependence of the AIE on the representation of the cloud water effect, we now calculate the AIE for a range of values of r_c in Representation 1 and of the cloud replenishment time scale τ_{rep} in Representation 2.

[52] Figure 7 shows that the dependence of the AIE on r_c is complex. The AIE is strongest for $r_c = 6$ μm, which according to equation (10) corresponds to $h_c = 0.5h$. For smaller but unrealistic values of r_c, the AIE is smaller in magnitude because the liquid water content of all but the thinnest clouds is determined by the product of the droplet number and the cube of r_c, which decreases rapidly as r_c decreases. This behavior is consistent with that found by *Rotstayn* [2000], *Menon et al.* [2002], and *Golaz et al*. [2011, 2013] using global models, except that in this simple model both the first and second indirect effect become small because as r_c approaches zero the cloud albedo approaches zero and hence the sensitivity of the cloud albedo to changes in effective radius is small [*Twomey*, 1991; *Platnick and Twomey*, 1994]. For r_c larger than 6 μm, the AIE in the simple model decreases with increasing r_c because more clouds are too thin for the droplet effective radius to exceed r_c. For r_c larger than 15 μm, the second indirect effect is negligible and the AIE saturates at the first indirect effect value. Typical values for r_c used in global models are 8–12 μm [*Rasch and Kristjansson*, 1998; *Rotstayn*, 2000; *Menon et al*., 2002; *Liu et al*., 2004; *Hsieh et al*., 2009; *Golaz et al*., 2011, 2013; *Rosenfeld et al*., 2012]. The

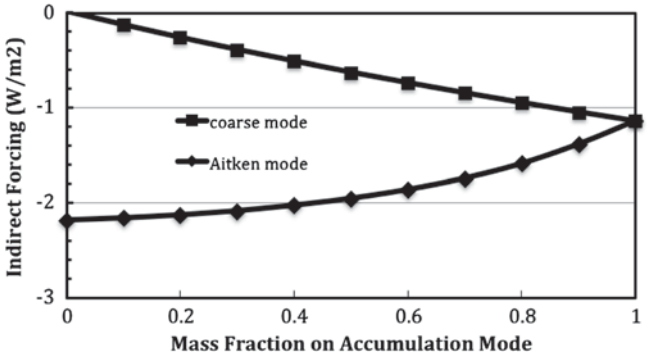

Figure 6. Indirect forcing for the CAM5 aerosol as a function of the mass fraction of the secondary anthropogenic aerosol applied to the accumulation mode, with the remainder distributed to the coarse mode (squares) and Aitken mode (diamonds). Other parameter values are baseline.

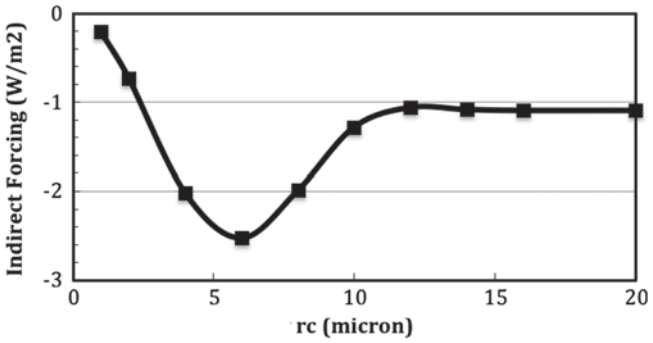

Figure 7. Indirect forcing as a function of the threshold radius for precipitation formation, r_c, using Representation 1 of the cloud water effect. All other parameters are baseline values.

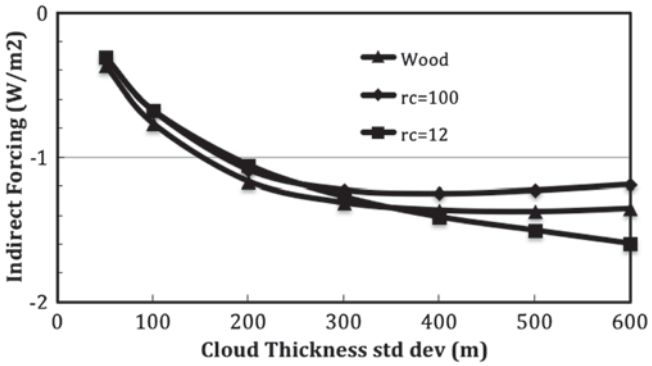

Figure 8. Indirect forcing as a function of the standard deviation of cloud thickness using the cloud water feedback Representation 2 (Wood) and Representation 1 with (r_c = 12 μm) and without (r_c = 100 μm) feedback.

different sensitivity of the AIE to critical radius in the global and simple models for this range of critical radius is likely due to the use of the PDF for cloud thickness in the simple model; none of the global models use a subgrid vertical PDF for clouds, and lack the vertical resolution to resolve such variability.

[53] For Representation 2 of the cloud water effect, the only poorly constrained parameter is the cloud replenishment time scale τ_{rep}. The simple model produces very little sensitivity of AIE to τ_{rep}, with AIE between −1.15 and −1.20 W m^{-2} for τ_{rep} between 600 and 14,400 s. These values of AIE are all within the range of AIE estimated with Representation 1 for the 8–12 μm range of r_c.

[54] Two processes increase the AIE with increasing standard deviation of cloud thickness (Figure 8). For narrow distributions, the forcing becomes stronger with increasing cloud thickness as the clouds become more susceptible to reductions in droplet effective radius. The susceptibility is greatest for clouds with albedos of 0.5 [*Twomey*, 1991; *Platnick and Twomey*, 1994]. For wider distributions, the indirect forcing continues to increase with increasing standard deviation as liquid water is influenced by the aerosol in more and more clouds, and the estimates with and without aerosol effects on cloud water diverge. For very high standard deviation, the albedo saturation effect takes over and limits the indirect forcing for clouds with albedo exceeding 0.5. This dependence is found for both representations of the cloud water effect, which yield similar estimates of the AIE for all but the largest cloud thickness standard deviations.

[55] As might be expected, the AIE is nearly proportional to low cloud fraction (not shown), varying from −0.73 W m^{-2} for f_c = 0.25 (the low cloud fraction estimated by ISCCP [*Rossow and Schiffer*, 1999]) to −1.29 W m^{-2} for f_c =0.4. Even if the baseline value is used for global mean cloud fraction, spatial correlations between cloud fraction and the anthropogenic aerosol burden can influence the AIE. For example, if the low cloud fraction simulated by CAM5 is averaged according to each of the ten equal-area bins used in the exponential frequency distribution of anthropogenic burden (scaled so the global mean low cloud fraction equals the baseline value), the negative correlation between simulated annual mean cloud fraction and anthropogenic burden leads to a reduction in AIE from −1.17 W m^{-2} to −0.99 W m^{-2}.

[56] AIE is remarkably insensitive to updraft velocity (Figure 9), even though droplet numbers vary by a factor of more than two as updrafts range from 10 to 100 cm s^{-1}. Part of the explanation for the insensitivity is that droplet numbers vary for preindustrial as well as present-day emissions. In addition, for low updraft velocities, the resulting small droplet number concentrations lead to a stronger the liquid water feedback. The AIE estimated with Representation 2 of the cloud water effect is very similar to that estimated with Representation 1.

[57] The AIE is also quite sensitive to the size distribution of the preindustrial aerosol. To see this, Figures 10–12 explore sensitivity of the forcing to the accumulation mode geometric standard deviation, the preindustrial number concentration, and mode radius, respectively. Since the Aitken and coarse modes of the CAM5 preindustrial aerosol do not greatly affect the indirect forcing estimate (the baseline estimate is −1.14 W m^{-2} without the Aitken and coarse modes, and −1.17 W m^{-2} with those modes), Figures 10–12 are based on estimates with all of the anthropogenic aerosol mass added to the accumulation mode.

[58] Figure 10 shows that the AIE is quite sensitive to the standard deviation of the size distribution, with forcing a factor 2.7 stronger for σ = 1.6 than for σ = 2.0. This can be explained in part by the smaller enhancement in aerosol number concentration and mode radius with increasing aerosol mass when σ is larger. In addition, the *Abdul-Razzak and*

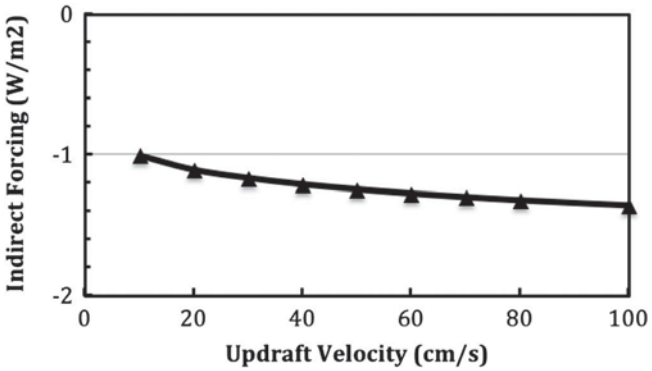

Figure 9. Indirect forcing as a function of updraft velocity.

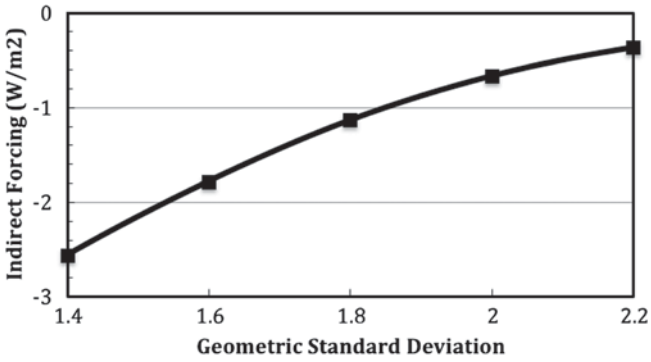

Figure 10. Indirect forcing as a function of geometric standard deviation for baseline anthropogenic emissions added to a single preindustrial aerosol mode with 0.071 μm number mode radius, 250 cm^{-3} number concentration and 0.36 hygroscopicity.

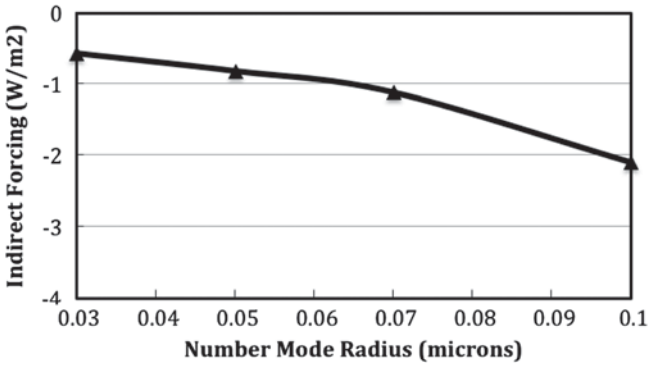

Figure 12. Indirect forcing as a function of number mode radius for an accumulation mode preindustrial aerosol with 1.8 geometric standard deviation, and 0.36 hygroscopicity and number concentration such that the volume is the same for all mode radii (equivalent to a number concentration of 250 cm^{-3} and number mode radius of 0.071 μm).

Ghan [2000] aerosol activation scheme decreases droplet nucleation as σ increases.

[59] Consistent with *Menon et al*. [2002] and *Chen and Penner* [2005], Figure 11 shows considerable sensitivity to the preindustrial aerosol number concentration, with the AIE increasing by a factor of 1.8 when preindustrial aerosol number decreases from 300 to 150 cm^{-3}.

[60] To isolate the dependence of the forcing on number mode radius, Figure 12 varies mode radius and N_n together such that the product $N_n r^3$ is unchanged. The forcing becomes more negative with increasing mode radius, as the number of preindustrial CCN decreases so that the primary emissions produce a relatively larger impact on droplet number. If primary emissions are neglected, the AIE asymptotes to a constant value for larger number mode radius (not shown). Differences between fixed and variable liquid water (r_c = 100 μm and r_c = 12 μm) (not shown) are significant only for mode radius larger than 0.07 μm, when aerosol and droplet number concentrations are small enough to produce droplets larger than r_c.

[61] The sensitivity tests are summarized in Figure 13, which shows the range in the AIE over the ranges in parameter values listed in Table 2 and estimates shown in Figures 4–12. Note that these simple sensitivity tests are from the baseline conditions. Sensitivities could be larger or smaller if starting from different conditions, as explored further below. There is a particularly large sensitivity (2.1 W m^{-2}) to the preindustrial aerosol number density, but uncertainty due to preindustrial accumulation mode radius as also very large. These large sensitivities indicate why reducing the uncertainty in the AIE has proven to be so difficult.

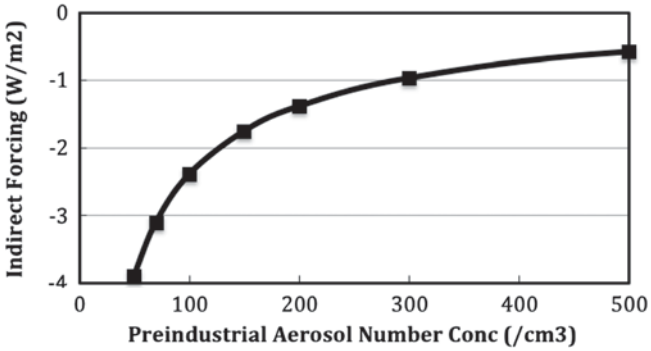

Figure 11. Indirect forcing as function of number concentration for an accumulation mode preindustrial aerosol with 0.071 μm number mode radius, 1.8 geometric standard deviation, and 0.36 hygroscopicity.

4. Testing With Global Aerosol Models

[62] We have found that the AIE depends on the size distribution of the preindustrial aerosol and on how the anthropogenic mass is distributed across the modes and between increasing mass and number. These distributions vary from model to model due to differences in preindustrial emissions, the representation of aerosol microphysics, and the treatment of aerosol transport and removal, so it is instructive to see how our method of distributing anthropogenic mass compares with the distribution simulated by various global aerosol models, and what the differences imply for the AIE. To do this, we compare estimates of indirect forcing using three methods: (A) this simple model using the simulated global mean preindustrial and present-day aerosol size distributions from several global aerosol models, with (B) this simple model with the simulated global mean preindustrial aerosol size distribution but distributing anthropogenic mass in proportion to preindustrial CCN concentration, and with anthropogenic emissions tuned to produce the same global mean present-day surface aerosol concentration as simulated by the global models, and (C) the indirect forcing estimate from the global model, where available. To permit a comparison with the same global burden of anthropogenic aerosol, we adjust the anthropogenic emissions so that the global mean anthropogenic aerosol mass concentration matches that from the global model simulation for the present-day conditions and consider a range of values of f_{new}. For estimate method A, we use equation (23) with the present-day and preindustrial number and mass concentrations to estimate f_{new} assuming the primary particles are at their emitted size. Method A is more likely to agree with method C because it uses more information from the global model, but method B permits studies with different emissions scenarios without

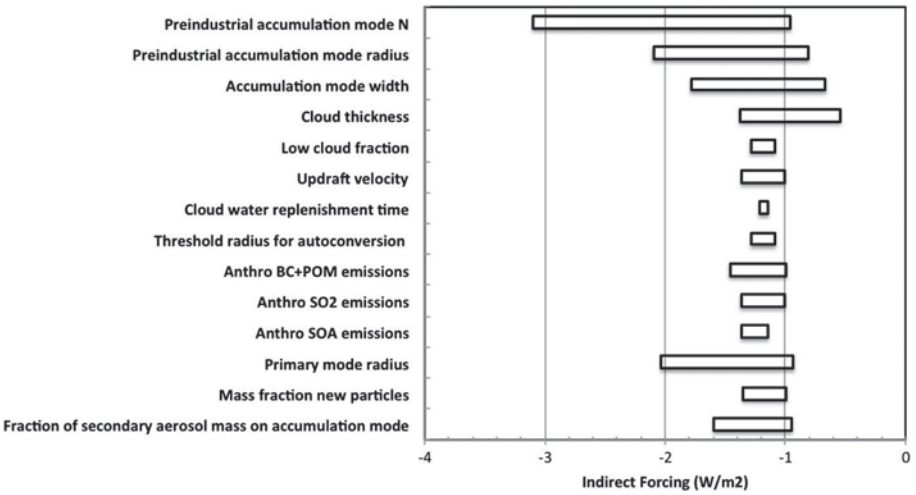

Figure 13. Range of indirect forcing estimates about baseline estimate for the plausible variations in model parameters listed in Table 2.

running the full aerosol model. Comparing methods A and B tests the validity of assuming that new mass is distributed across modes in proportion to preindustrial CCN concentration.

4.1. CAM5

[63] The baseline case examined previously has parameters drawn from the CAM5 model. The anthropogenic sulfur emission that, using the prescribed aerosol lifetime and scale height in this simple model, produces the same global mean anthropogenic sulfate mass concentration as simulated by CAM5 is 95 Tg/yr, which is less than the 110 Tg/yr anthropogenic sulfur emission used in the CAM5 simulation, and the anthropogenic SOA emission that produces the same anthropogenic SOA concentration in the CAM5 simulations is 25 Tg/yr, more than the 14 Tg/yr SOA emission in the CAM5 simulation, for a total secondary aerosol emission of 120, only slightly less than the 124 Tg/yr secondary anthropogenic emission used in the CAM5 simulation. The primary emission that produces the same global mean anthropogenic primary mass concentration as simulated by CAM5 is 38 Tg/yr, which is much more than the 22 Tg/yr in the CAM5 simulations, because of differences between the prescribed scale height and aerosol lifetime and those in the simulation (the scale height of sulfate is 50% greater than for primary material because SO_2, the precursor gas of sulfate, can be transported upward more easily than aerosol). These emissions yield indirect forcing estimates of -1.08 and -1.60 W m^{-2} for $f_{new}=0$ and $f_{new}=1$, respectively, using method B, which span the -1.52 W m^{-2} forcing estimated by method A using the preindustrial and present-day CAM5 aerosol size distributions (which using equation (23) diagnoses $f_{new}=0.86$ for the accumulation mode). This suggests that distributing anthropogenic mass across modes using the preindustrial mode distribution works well for CAM5. However, these estimates of the AIE are still 25% smaller than that estimated by the full CAM5 physics (method C), about -2.0 W m^{-2} [*Ghan et al*., 2012].

4.2. MMF

[64] Figure 14 shows the AIE as a function of f_{new}, using method B with the preindustrial aerosol size distributions from the Multiscale Modeling Framework (MMF) model (Table 3), which is a version of CAM with an embedded two-dimensional cloud model used to represent clouds and their interactions with aerosols [*Wang et al*., 2011]. With method B, the sulfur, SOA, and primary anthropogenic emissions are diagnosed to be 112, 19, and 34 Tg/yr, respectively, which are comparable to the estimates for CAM5. The AIE estimated with method B is -1.10 and -1.69 W m^{-2} for $f_{new}=0$ and 1, respectively, which span the method A estimate: -1.40 W m^{-2}. The estimates are similar to those for CAM5, which is to be expected because the aerosol microphysics is identical (though the influence of clouds on the aerosol is quite different in the two models), and hence the preindustrial size distributions, CCN concentrations, and anthropogenic emissions are similar. The indirect forcing estimated by the full MMF is -0.77 W m^{-2} [*Wang et al*., 2011], which is half of the method A estimate by the simple model, and significantly smaller than that estimated by the full CAM5. Thus, the simple model is unable to explain the nearly threefold difference between the indirect forcing estimated by CAM5 and the MMF. *Wang et al*. [2011] concluded that differences in the liquid water path response of the two models is responsible for most of the difference

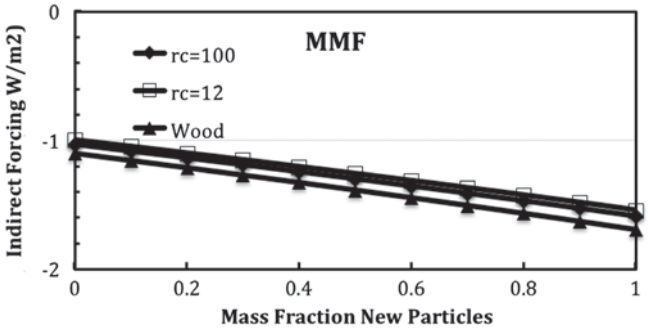

Figure 14. Indirect forcing estimated using method B for MMF aerosol using Representation 1 of aerosol effects on cloud liquid water ($r_c=12$ μm), neglecting aerosol effects on cloud water ($r_c=100$ μm), and using Representation 2 of aerosol effects on cloud liquid water (Wood).

Table 3. Global Mean Surface Values of the MMF Aerosol

Mode	Preindustrial	Present Day
	Aitken	
N (# cm^{-3})	195	256
r_n (μm)	0.016	0.017
σ	1.6	1.6
CCN(0.2%) (# cm^{-3})	5	8
q_{sulf} (μg m^{-3})	0.014	0.022
q_{SOA} (μg m^{-3})	0.000	0.000
$q_{seasalt}$ (μg m^{-3})	0.003	0.003
	Accumulation	
N (# cm^{-3})	275	395
r_n (μm)	0.065	0.064
σ	1.8	1.8
CCN(0.2%) (# cm^{-3})	169	240
q_{sulf} (μg m^{-3})	0.46	1.24
q_{SOA} (μg m^{-3})	0.69	0.82
q_{BC} (μg m^{-3})	0.03	0.08
q_{POM} (μg m^{-3})	0.32	0.52
q_{dust} (μg m^{-3})	1.19	1.19
$q_{seasalt}$ (μg m^{-3})	0.69	0.69
	Coarse	
N (# cm^{-3})	1.39	1.35
r_n (μm)	0.778	0.773
σ	1.8	1.8
CCN(0.2%) (# cm^{-3})	1.4	1.4
q_{sulf} (μg m^{-3})	0.01	0.03
q_{dust} (μg m^{-3})	19.2	19.2
$q_{seasalt}$ (μg m^{-3})	12.4	12.4
Total CCN(0.2%) (# cm^{-3})	176	249

Table 4. Global Mean Surface Values for the Soluble Modes of the ECHAM5-HAM Aerosol

Mode	Preindustrial	Present Day
	Aitken	
N (# cm^{-3})	292	313
r_n (μm)	0.013	0.015
σ	1.59	1.59
CCN(0.2%) (# cm^{-3})	2	3
q_{sulf} (μg m^{-3})	0.011	0.011
q_{SOA} (μg m^{-3})	0.001	0.001
q_{BC} (μg m^{-3})	0.000	0.001
q_{POM} (μg m^{-3})	0.003	0.005
	Accumulation	
N (# cm^{-3})	87	180
r_n (μm)	0.083	0.089
σ	1.59	1.59
CCN(0.2%) (# cm^{-3})	79	161
q_{sulf} (μg m^{-3})	0.33	1.05
q_{SOA} (μg m^{-3})	0.08	0.16
q_{BC} (μg m^{-3})	0.01	0.06
q_{POM} (μg m^{-3})	0.13	0.49
q_{dust} (μg m^{-3})	0.06	0.06
$q_{seasalt}$ (μg m^{-3})	0.66	0.66
	Coarse	
N (# cm^{-3})	1.68	1.9
r_n (μm)	0.520	0.507
σ	2.0	2.0
CCN(0.2%) (# cm^{-3})	2	2
q_{sulf} (μg m^{-3})	0.03	0.06
q_{SOA} (μg m^{-3})	0.00	0.00
q_{BC} (μg m^{-3})	0.00	0.00
q_{POM} (μg m^{-3})	0.00	0.00
q_{dust} (μg m^{-3})	2.11	2.11
$q_{seasalt}$ (μg m^{-3})	16.2	16.2
Total CCN(0.2%) (# cm^{-3})	83	166

in the indirect forcing. In the simple model as shown in Figure 14, the liquid water feedback makes little difference in the AIE. However, as shown in Figure 8, the liquid water feedback in the simple model can be important for thicker clouds. While *Wang et al*. [2012] suggest that differences in the treatment of rain in CAM5 and the MMF cause the weaker liquid water feedback in the MMF, perhaps it is also due to differences in cloud thickness.

4.3. ECHAM5-HAM

[65] The global mean surface aerosol parameters for the ECHAM5-HAM aerosol model [*Stier et al*., 2005; *Zhang et al*., 2012] are listed in Table 4. Using these parameters, the global anthropogenic sulfur, SOA, and primary emissions estimated with this model are 104, 12, and 59 Tg/yr, respectively. The secondary emissions are similar for CAM5, reflecting the comparable anthropogenic secondary aerosol concentrations in the ECHAM5-HAM aerosol simulations. On the other hand, the ECHAM5-HAM primary anthropogenic emissions diagnosed by this model are 58% greater than those for CAM5, as the anthropogenic BC and POM concentrations simulated by ECHAM5-HAM are nearly double those simulated by CAM5, reflecting much longer lifetimes rather than shorter scale heights for BC and POM in ECHAM5-HAM.

[66] As shown in Figure 15, the AIE estimated with $r_c = 12$ μm using method B and Representation 2 of the cloud water effect is -4.1 Wm^{-2} for $f_{new} = 0$ and -5.4 Wm^{-2} for $f_{new} = 1$. These estimates with secondary material distributed in proportion to preindustrial CCN concentration (method B) are somewhat larger than the AIE estimated directly using the ECHAM5-HAM present-day and preindustrial global mean concentrations (method A): -3.9 Wm^{-2}. This suggests that distributing secondary material in proportion to preindustrial CCN concentration also works well for compared to the distribution simulated by ECHAM5-HAM. As in CAM5, the vast majority of the anthropogenic mass goes on the accumulation mode under this assumption. However, the indirect forcing thus estimated is about three to four times as large as with the CAM5 preindustrial aerosol for the same f_{new} and emissions. The much larger forcing is partly due to the larger anthropogenic primary aerosol and partly due to the nearly threefold smaller preindustrial aerosol accumulation mode aerosol concentration in ECHAM5-HAM as compared with CAM5. The preindustrial CCN concentration, listed in Table 4, is consequently a factor of more than two smaller. The anthropogenic aerosol therefore has a much larger

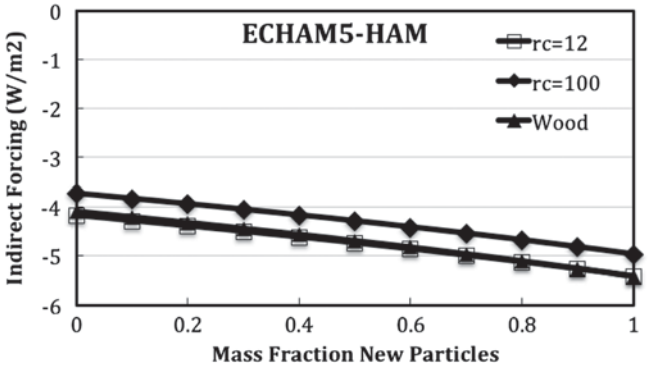

Figure 15. As in Figure 14, but for the ECHAM5-HAM aerosol.

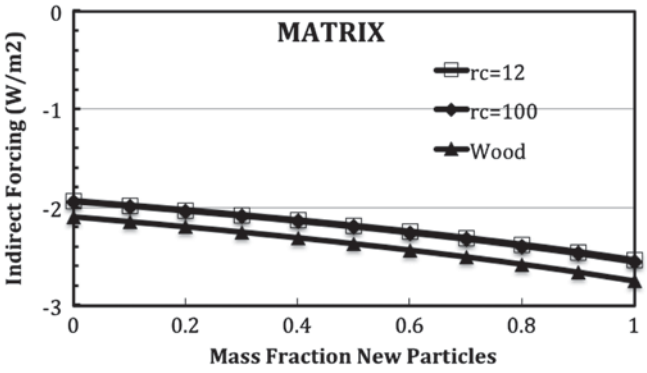

Figure 16. As in Figure 14, but for MATRIX aerosol.

influence on the accumulation mode aerosol number for ECHAM5-HAM case compared with CAM5.

[67] Since the AIE from the simple model for ECHAM5-HAM preindustrial aerosol parameters is much larger than the forcing estimates for CAM5, one might expect the AIE estimated directly from full ECHAM5-HAM simulations would be much larger than that estimated from CAM5 simulations. In fact, the estimate from ECHAM5-HAM simulations is *smaller*, −1.2 versus −2.0 W m^{-2} (K. Zhang, personal communication, 2012).

[68] Why is the ECHAM5-HAM indirect forcing so much smaller than the simple model estimates with methods A or B? Turning off the liquid water feedback in the simple model reduces the indirect forcing to −3.6 W m^{-2} with method A, so if the simple model overestimates the liquid water feedback that would explain part of the difference. The radius of the primary particles might be larger than the 0.05 μm radius assumed here, though particles produced from fossil fuel combustion in the ECHAM5-HAM are emitted at a smaller radius (0.03 μm) than in CAM5. Even if the radius of the primary particles r_{prim} is assumed to be 0.08 μm in the simple model the indirect forcing without liquid water feedback and $f_{new}=0$ is estimated to be −1.8 W m^{-2}. The 20 cm^{-3} droplet number minimum in ECHAM5-HAM might play role in that model [*Lohmann et al*., 2007; *Hoose et al*., 2009], but we have found that it makes little difference in this simple model because preindustrial droplet number concentrations are uniformly much higher than 20 cm^{-3}. The global mean low cloud fraction simulated by ECHAM-HAM is close to that estimated from CALIPSO. Negative spatial and temporal correlations between cloud and anthropogenic aerosol simulated by ECHAM5-HAM could contribute to the difference, but when the CAM5 spatial correlations are applied to ECHAM5-HAM, the AIE is further diminished to −1.5 W m^{-2}, which is comparable to that estimated from full ECHAM5-HAM simulations. However, this level of agreement is only achieved through neglecting the cloud water effect and using unrealistic values for f_{new} and r_{prim}. Thus, the large magnitude of the AIE estimated by the simple model is not easily reconciled with the estimate by full ECHAM5-HAM simulations.

4.4. GISS-MATRIX

[69] The Goddard Institute for Space Studies Multiconfiguration Aerosol TRacker of mIXing state (GISS-MATRIX) aerosol model [*Bauer et al*., 2008] tracks aerosols depending on mixing state classes and hence distinguishes many more aerosol modes than CAM5, MMF, or ECHAM5-HAM. Anthropogenic emissions needed for the simple model to produce the simulated preindustrial to present-day increase in global mean surface concentrations are 71 Tg/yr for sulfur, 11 Tg/yr for SOA, and 23 Tg/yr for primary. Figure 16 shows the AIE as a function of f_{new} for method B using aerosol parameters from the MATRIX model listed in Table 5 (modes that contribute little to the aerosol number or surface area are omitted). Since the MATRIX history

Table 5. Global Annual Mean Surface Values of the GISS-MATRIX Aerosol

Mode	Preindustrial	Present Day
	Sulfate Aitken	
N (# cm^{-3})	3241	17,110
r_n (μm)	0.003	0.002
σ	1.6	1.6
CCN(0.2%) (# cm^{-3})	0.3	0.5
q_{sulf} (μg m^{-3})	0.002	0.004
	Sulfate accumulation	
N (# cm^{-3})	781	700
r_n (μm)	0.017	0.021
σ	1.8	1.8
CCN(0.2%) (# cm^{-3})	41.5	59.8
q_{sulf} (μg m^{-3})	0.14	0.21
	Organic carbon	
N (# cm^{-3})	810	969
r_n (μm)	0.027	0.029
σ	1.8	1.8
CCN(0.2%) (# cm^{-3})	63.5	119
q_{sulf} (μg m^{-3})	0.14	0.32
q_{SOA} (μg m^{-3})	0.46	0.53
	BC-sulfate	
N (# cm^{-3})	9.2	44.5
r_n (μm)	0.029	0.033
σ	1.8	1.8
CCN(0.2%) (# cm^{-3})	0.3	3.9
q_{sulf} (μg m^{-3})	0.001	0.014
q_{BC} (μg m^{-3})	0.007	0.040
	BC-OC-sulfate	
N (# cm^{-3})	50	94
r_n (μm)	0.048	0.054
σ	1.8	1.8
CCN(0.2%) (# cm^{-3})	8.5	36.5
q_{sulf} (μg m^{-3})	0.037	0.24
q_{POM} (μg m^{-3})	0.14	0.26
q_{BC} (μg m^{-3})	0.02	0.03
	Mixed	
N (# cm^{-3})	1.66	1.76
r_n (μm)	0.67	0.67
σ	1.8	1.8
CCN(0.2%) (# cm^{-3})	1.66	1.76
q_{sulf} (μg m^{-3})	0.033	0.058
q_{SOA} (μg m^{-3})	0.002	0.002
q_{BC} (μg m^{-3})	0.000	0.000
q_{dust} (μg m^{-3})	14.3	14.3
$q_{seasalt}$ (μg m^{-3})	9.9	9.9
	Sea salt accumulation	
N (# cm^{-3})	7.4	7.2
r_n (μm)	0.185	0.185
σ	1.8	1.8
CCN(0.2%) (# cm^{-3})	7.3	7.1
$q_{seasalt}$ (μg m^{-3})	2.27	2.27
	Sea salt coarse	
N (# cm^{-3})	0.005	0.005
r_n (μm)	1.96	1.96
σ	2.0	2.0
CCN(0.2%) (# cm^{-3})	0.005	0.005
$q_{seasalt}$ (μg m^{-3})	5.6	5.6
Total CCN(0.2%) (# cm^{-3})	123	229

Table 6. Global Mean Surface Values of the UKCA Aerosol

Mode	Preindustrial	Present Day
	Soluble Aitken	
N (# cm^{-3})	38.3	112
r_n (μm)	0.038	0.041
σ	1.59	1.59
CCN(0.1%) (# cm^{-3})	9.9	38
q_{sulf} (μg m^{-3})	0.04	0.11
q_{om} (μg m^{-3})	0.007	0.053
q_{BC} (μg m^{-3})	0.00	0.008
	Accumulation	
N (# cm^{-3})	58.3	92.0
r_n (μm)	0.10	0.10
σ	1.59	1.59
CCN(0.1%) (# cm^{-3})	56	87
q_{sulf} (μg m^{-3})	0.33	1.03
q_{om} (μg m^{-3})	0.24	0.28
q_{BC} (μg m^{-3})	0.01	0.02
$q_{seasalt}$ (μg m^{-3})	0.91	0.91
	Soluble coarse	
N (# cm^{-3})	4.7	4.7
r_n (μm)	0.685	0.685
σ	2.0	2.0
CCN(0.1%) (# cm^{-3})	4.69	4.69
$q_{seasalt}$ (μg m^{-3})	13.9	13.9
Total CCN(0.1%) (# cm^{-3})	70	129

lumps primary and SOA, we have assumed all organic aerosol is secondary except for the BC-OC-sulfate mode, for which we assume all organic is primary. The AIE from method B ranges from −2.1 to −2.8 W m^{-2} for Representation A of the cloud water effect, which does not quite span the method A estimate: −2.0 W m^{-2}. There is little dependence on whether the liquid water feedback is included. These estimates are comparable to the estimates for CAM5 and MMF aerosol, but are much larger than the estimate of the first AIE by the full GISS-MATRIX model [*Bauer and Menon*, 2012]: −0.17 W m^{-2}. This simple model is not capable of producing such a small estimate unless the cloud fraction is decreased considerably. However, the low cloud cover simulated by GISS-modelE, the MATRIX host model, is 36%, close to the CALIPSO value used in the simple model. Very strong anticorrelation between cloud cover and anthropogenic aerosol must be invoked to fully explain the difference.

[70] We therefore find mixed results for the four models for which we have values for the AIE. The simple model can match well the somewhat high value from CAM5. The simple model is twice the AIE in the MMF model. The simple model predicts a much higher AIE than reported for either the ECHAM5-HAM or GISS-MATRIX models for reasons that are not clear. Some mechanism in these models reduces the AIE below the value that would otherwise be expected. It is likely that clouds and aerosols simulated by the full models are negatively correlated, so the neglect of that correlation in the simple model could explain the difference in the estimated AIE. Further analysis of the correlations in each of the full models is needed to determine why the difference is large for some models but small for others. It is also possible that the application of a minimum droplet number in the ECHAM5-HAM and GISS-MATRIX models but not in CAM5 or the MMF could also play an important role. *Quaas et al*. [2009] found a significant correlation between indirect forcing estimates by global models and the droplet number minimum. Such a minimum is more likely to be important in the former models because of their relatively low preindustrial CCN concentrations. Although applying a minimum droplet number to the simple model made little difference, it could be more important in the full models, which represent temporal variability in droplet number, which is neglected in the simple model.

4.5. UKCA

[71] The AIE estimated using aerosol concentrations from the UKCA model [*Mann et al*., 2010] depends strongly on how much of the organic aerosol is primary or secondary. The UKCA simulates aerosol with seven modes. Table 6 lists the global mean surface concentrations of the components of three of the seven UKCA modes (the nuclei and the three insoluble modes do not influence the AIE and hence are neglected; dust is not simulated). It lumps all organic aerosol together, so the partitioning of secondary and primary organic concentrations is not known. According to Tables 1, 3, 4, and 5, the fraction of the accumulation mode organic aerosol that is secondary ranges from 25% for ECHAM5 to 68% for CAM5 and MMF. Figure 17 shows the AIE as a function of f_{new}, using the preindustrial aerosol size distributions from the UKCA model, estimated using method B and Representations 1 and 2 with and without cloud liquid water feedback, assuming all organic is either primary or secondary. The AIE is less than −2 W m^{-2} if all organic is secondary and a small fraction of the secondary aerosol forms new particles. Liquid water feedback nearly doubles the AIE for all conditions; if a small fraction of the secondary aerosol forms new particles, then assuming all organic aerosol is primary nearly doubles the AIE again. As might be expected, the partitioning of organic aerosol makes less of a difference if most of the secondary material is assumed to produce new particles. Method A also reveals considerable sensitivity to liquid water feedback, with the AIE increasing 50% with feedback, for either organic aerosol assumed to be primary (−2.5 to −3.7 W m^{-2}) or secondary (−2.2 to −3.3 W m^{-2}). But the AIE increases by only about 15% when organic aerosol is assumed to be primary rather secondary. This is to

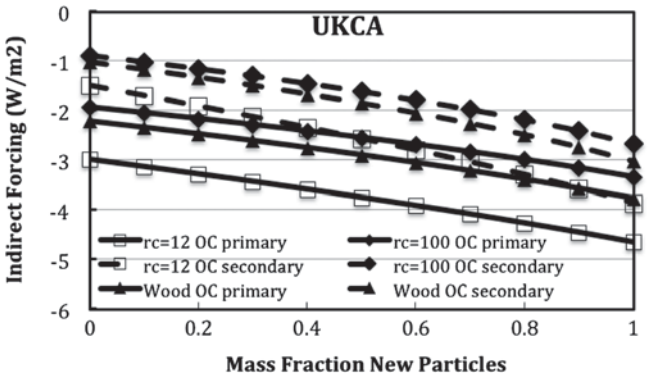

Figure 17. Indirect forcing estimated using method B for UKCA aerosol using Representation 1 of aerosol effects on cloud liquid water (r_c = 12 μm), neglecting effects on cloud water (r_c = 100 μm), and using Representation of aerosol effects on cloud liquid water, assuming all organic aerosol is primary (solid lines) or secondary (dashed lines).

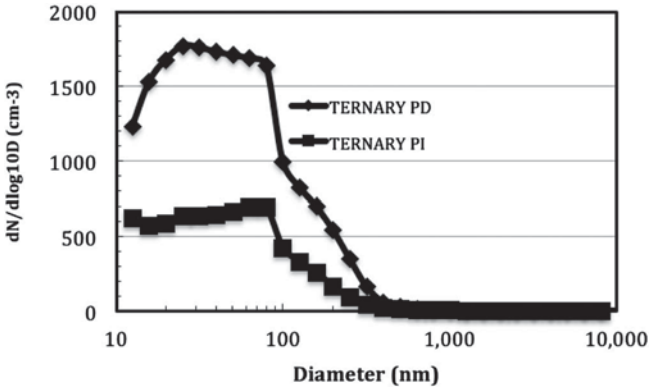

Figure 18. Global and annual mean preindustrial (PI) and present-day (PD) aerosol size distributions simulated by TOMAS with a ternary homogeneous nucleation scheme [*Pierce and Adams*, 2009].

be expected, because with method A, the partitioning of primary and SOA does not influence the anthropogenic increase in number for each mode. In all cases, the AIE estimated by method A falls within the range of method B estimates for $f_{new} = 0$ to 1.

4.6. GISS-TOMAS

[72] The simple model can be applied to even more complex representations of the aerosol. Figure 18 shows the global mean present-day and preindustrial aerosol size distribution in the lowest layer of the GISS TwO-Moment Aerosol Sectional (GISS-TOMAS) model [*Pierce et al*., 2007; *Pierce and Adams*, 2009], which simulates sulfate, sea salt, BC, and organic carbon but not mineral dust in each of 30 size bins. Seventy percent of the total anthropogenic mass in the GISS-TOMAS simulations is sulfate, but the sulfate fraction varies with size from 5% to 100%. These simulations use the *Napari et al*. [2002] ternary nucleation scheme, which is known to overpredict nucleation rates. Therefore, these simulations likely have too many nucleation and Aitken-mode particles for both the PI and PD simulation. However, this case is used to represent the application of the AIE-prediction method to a sectional aerosol model. To apply the Abdul-Razzak scheme to diagnose droplet nucleation for the GISS-TOMAS sectional representation of the aerosol, we have expressed the 30 sections of GISS-TOMAS as 30 lognormal modes, with standard deviations given by

$$\sigma = \exp\left(0.5\ln\left({}^{r_+}/_{r_-}\right)\right)$$

where r_+ and r_- are the radii at the upper and lower boundaries of the sections. For a sectional model, a single value for the size of primary particles cannot apply to all sections, so we assume the primary particle radius to be the central value of the section. Figure 19 shows the AIE as a function of f_{new}, using method B and the aerosol size distributions from the GISS-TOMAS model. Surprisingly, the AIE decreases as f_{new} increases. This occurs because, even though aerosol number in each bin increases, the particle radius decreases enough to influence droplet nucleation more than the increase in aerosol number. Unlike estimates for modal models, the ranges of the AIE estimated using method B for all treatments of liquid water feedback shown in

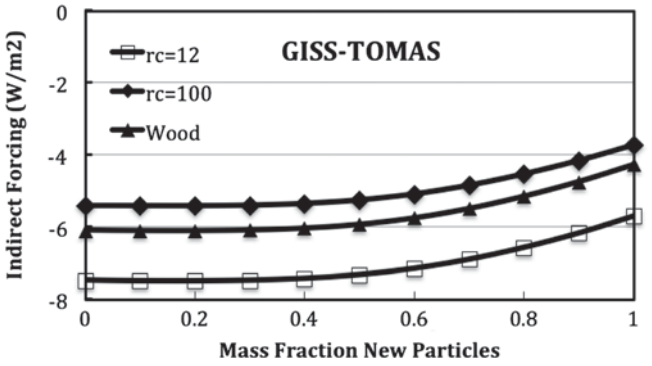

Figure 19. As in Figure 14, but for GISS-TOMAS aerosol.

Figure 19 exceed the estimates with method A: -5.4 W m^{-2}, -3.6 W m^{-2}, and -4.1 W m^{-2} for Representation 1 with r_c = 12 and 100 μm and for Representation 2, respectively, for all values of f_{new}. This suggests the method of distributing secondary anthropogenic aerosol mass in proportion to preindustrial CCN concentration does not work so well for the GISS-TOMAS sectional model. Indeed, the AIE estimates with method B are sensitive to the supersaturation used to determine CCN. Supersaturation values higher than the 0.2% value used in this model yield more positive method B estimates of AIE, as more of the secondary anthropogenic mass is distributed to smaller bins that are too small to form droplets. The estimates are larger than those from other models because of the fourfold anthropogenic increase in CCN concentration, from a relatively low value of 79 cm^{-3} for preindustrial emissions to 276 cm^{-3} for present-day emissions. Liquid water feedback influences the AIE more because of the low preindustrial CCN concentration. The anthropogenic emissions that are consistent with the anthropogenic global mean surface mass concentration are consequently unrealistically large: 168 Tg/yr secondary and 91 Tg/yr primary. The scale height of anthropogenic aerosol simulated by GISS-TOMAS is 2.6 km, smaller than the 3 km value in the simple model. This suggests a much longer anthropogenic aerosol lifetime in the GISS-TOMAS simulations than the assumed 4 day lifetime in the simple model.

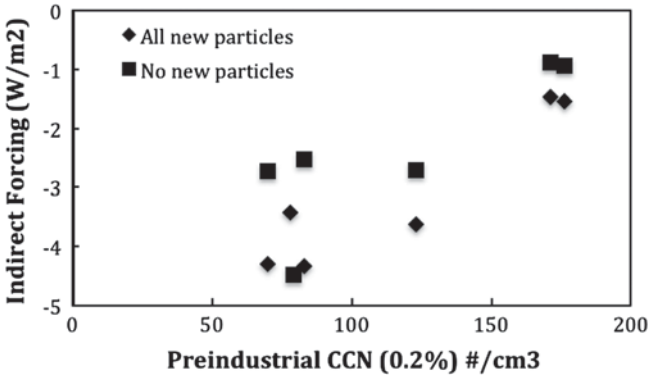

Figure 20. Indirect forcing estimated with the baseline emissions, $f_{new} = 0$ (squares) and $f_{new} = 1$ (diamonds), for preindustrial aerosol parameters from global means of each global aerosol model, plotted versus the preindustrial CCN concentration for those models. All other model parameters are baseline values.

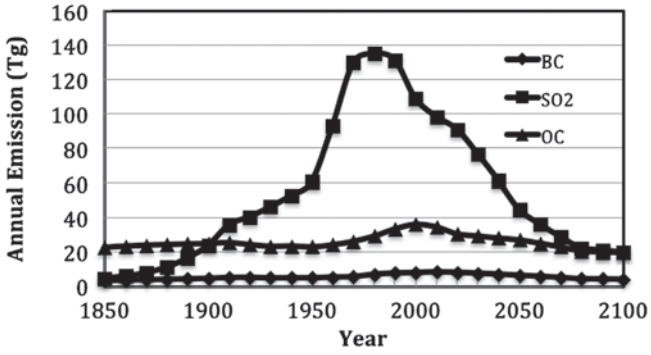

Figure 21. Global mean annual emissions of SO_2, BC, and OC from historical estimates [*Lamarque et al*., 2010] and (for 2000 to 2100) from RCP 4.5 [*Thomson et al*., 2011].

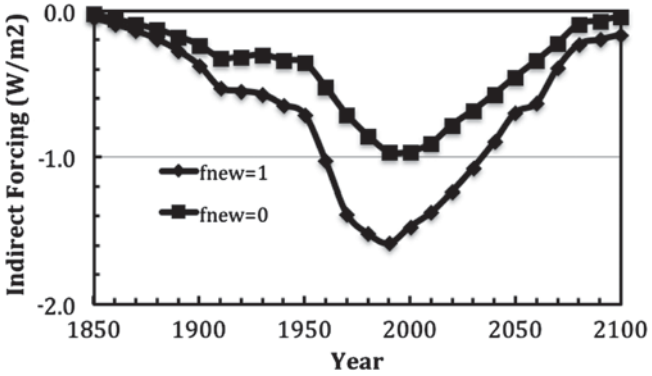

Figure 22. Indirect forcing estimated for historical and RCP 4.5 emissions of anthropogenic SO_2, BC, and OC shown in Figure 21, using the CAM5 preindustrial aerosol size distribution, Representation 2 of the cloud water effect, and $f_{new} = 1$ (diamonds) and $f_{new} = 0$ (squares).

Indeed, *Pierce et al*. [2007] find that the GISS-TOMAS model produces lifetimes of 6, 5.5, and 8.5 days for sulfate, OC, and BC, respectively.

4.7. Global Aerosol Model Summary

[73] These comparisons suggest that the distribution of secondary anthropogenic mass across modes using preindustrial CCN concentration works well for most models but not for those that add significant anthropogenic mass to finer or coarser modes (i.e., the size distribution shifts to smaller or larger sizes). The intermodel differences in anthropogenic aerosol mass are surprisingly large and contribute to the large differences in the indirect forcing estimated using the global mean preindustrial aerosol size distributions from the different models. As shown in Figure 20, differences in preindustrial aerosol size distributions produce most of the diversity in AIE estimates when anthropogenic aerosol is determined by baseline emissions, with much stronger AIE when preindustrial CCN concentration is low. These differences in preindustrial CCN likely depend on uncertain aspects of the aerosol models such as the treatment of wet removal. Liquid water feedback plays an important role if preindustrial aerosol concentrations are low or if the droplet threshold for autoconversion is smaller than the baseline value. Emissions of primary anthropogenic aerosol are important if the primary particle mode radius is less than 0.08 μm and little of the secondary anthropogenic aerosol forms new particles. Because different models use different numbers of modes and assume different mode widths, it is not possible to combine the different natural and anthropogenic aerosol results into a single composite model with a range of parameter values. The indirect forcing values exceeding 4 W m^{-2} in cooling are clearly inconsistent with observationally estimated constraints on total aerosol forcing [e.g., *Murphy et al*., 2009].

5. Application to Future Forcing

[74] A primary purpose for a simple representation of the AIE is application to future emissions scenarios. Figure 21 shows global emissions of SO_2, BC, and POM estimated for 1850–2000 by *Lamarque et al*. [2010] and projected to 2100 for the RCP4.5 emissions scenario by *Thomson et al*. [2011]. In this scenario, global SO_2 emissions decline from 110 Tg SO_2 in 2000 to 20 Tg SO_2 in 2100, while emissions of BC and OC decrease by about 50%. Simple parameterizations used in IAMs result in estimates 2100 AIE that are 45 – 70% lower in 2100 than 2000, depending on the parameterization used [*Thomson et al*., 2011; *Meinshausen et al*., 2011b]. Such a fractional reduction is much smaller than the 82% reduction in SO_2 emissions, because those parameterizations assume a logarithm dependence of the AIE on aerosol. Here we use the simple model to show a much more linear response. We find (Figure 22) that, using the baseline parameter values, Representation 2 of the liquid water feedback and subtracting the 1850 primary emissions to determine the anthropogenic primary emissions, the AIE for the RCP4.5 emissions in 2100 is 88–95% smaller than that at 2000. This is a much larger fractional reduction in forcing than the 56% reduction from the previous widely used logarithmic representation [*Wigley and Raper*, 1992] and exceeds the fractional reduction in SO_2 emissions because the primary emissions in 2100 in this scenario are projected to be less than the 1850 emissions, so that the reduction in primary emission exceeds 100%. This produces a much more linear response of AIE to emissions, illustrated in Figure 23, than

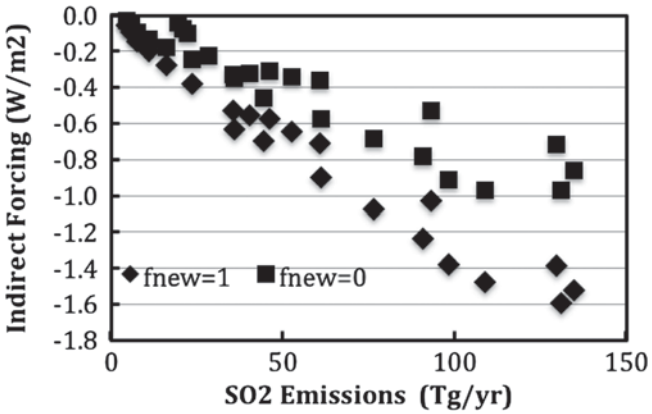

Figure 23. Relationship between AIE and SO2 emissions for historical and RCP 4.5 emissions of anthropogenic SO_2, BC and OC shown in Figure 21, using the CAM5 preindustrial aerosol size distribution, Representation 2 of the cloud water effect, and $f_{new} = 1$ (diamonds) and $f_{new} = 0$ (squares).

the logarithmic model produces. For a more aggressive emissions reduction scenario such as GCAM2.6 [*Thomson et al*., 2011], which reduces sulfur, BC, and OC emissions in 2095 to 10, 2, and 16 Tg/yr, respectively, the AIE is +0.16 W m^{-2}, the positive value clearly demonstrating the importance of the reduction in the primary emissions to values below those for year 1850. Clearly, comparisons with indirect aerosol forcing estimates from full global aerosol models are needed for these emissions scenarios.

6. Conclusions

[75] To summarize, the parametric uncertainty in the estimated AIE (Figure 13) is greatest for the preindustrial accumulation mode number concentration, then the mean radius of the preindustrial accumulation mode aerosol (assuming the mass is known), followed by the accumulation mode width, and then the size of the primary particles. Significant uncertainty also arises due to uncertainty in the primary carbonaceous and secondary sulfur anthropogenic emissions (the latter is uncertain because of uncertainty in sulfate production, not uncertainty in SO_2 emission), cloud thickness through its influence on the liquid water feedback, the fraction of the secondary anthropogenic emissions that accumulates on the coarse mode, the fraction of the secondary mass that forms new CCN-size particles, the cloud distribution, and the critical size for autoconversion of cloud droplets. The forcing is relatively insensitive to the updraft velocity, the cloud water replenishment time, and SOA production. The relative importance of each of these parameters depends on the values of the other parameters. For example, the fraction of the secondary mass that forms new particles is less important if primary particles dominate the CCN concentration, and the uncertainty due to the liquid water feedback is much greater when preindustrial CCN concentration is low. The parametric dependence is similar to that found by studies using much more complete global aerosol models [*Rotstayn*, 2000; *Menon et al*., 2002; *Adams and Seinfeld*, 2003; *Chen and Penner*, 2005; *Haerter et al*., 2009; *Storelvmo et al*., 2009; *Pierce and Adams*, 2009; *Lohmann and Ferrachat*, 2010; *Lee et al*., 2011, 2013; *Reddington et al*., 2011]. Although droplet number increases sublinearly with aerosol number and cloud albedo increases sublinearly with optical depth, the AIE is surprisingly linear in SO_2 emissions. This finding should be tested with forcing estimates by full global aerosol models for different emissions scenarios.

[76] The large contribution of uncertainty in preindustrial aerosol to uncertainty in the estimated indirect forcing has been found by others [*Storelvmo et al*., 2009; K. S. Carslaw personal communication, 2013]. The implication for this finding is that it is important to validate aerosol models in relatively pristine regions that might be representative of preindustrial conditions. All important natural sources of CCN need to be treated.

[77] The simple model produces a wide range in estimates of present-day-preindustrial AIE. For baseline anthropogenic emissions and CAM5 preindustrial aerosol, AIE values as small as -0.3 Wm^{-2} are estimated when only a small fraction of secondary aerosol produces new particles ($f_{new} = 0.2$), a significant fraction (20%) of the secondary material condenses on the coarse mode, primary particles coagulate to the same size as accumulation mode particles ($r_{prim} = 0.07$ μm), the accumulation mode size distribution is broader ($\sigma = 2.0$), the preindustrial CCN concentration is high (250 cm^{-3}), and cloud liquid water path does not respond to droplet number changes ($r_c = 100$ μm). Values as large as -5 Wm^{-2} are estimated when all secondary aerosol produces new particles ($f_{new} = 1$), all of the secondary material forms accumulation mode aerosol, the primary particles do not coagulate ($r_{prim} = 0.04$ μm), the size distribution is narrow ($\sigma = 1.6$), the preindustrial CCN concentration is low (100 cm^{-3}), and cloud liquid water path increases with droplet number ($r_c = 12$ μm).

[78] The forcing estimates based on the assumption that anthropogenic mass can be distributed in proportion to CCN concentration work better than distribution in proportion to number or surface area. For most global aerosol models the distribution assumption produces indirect forcing in good agreement with estimates using the distribution of anthropogenic mass and number simulated by global aerosol models, but for some models it does not.

[79] For three out of four of the full aerosol models for which we have estimates of the AIE, the baseline parameter values in the simple model produce much larger estimates of the AIE than the full models produce, given the preindustrial and present-day distributions of the aerosol from the full models. Only a few combinations of plausible values in parameters of the simple model can produce estimates as small as those estimated by some of the full models. Further examination of the reasons for the smaller AIE in these models would provide insights into the reasons for the wide variation in model-based AIE estimates and would help improve simple models such as the one presented here.

[80] There are other limitations of this simple model. It assumes cloud fraction is uncorrelated with anthropogenic aerosol, but since precipitation from clouds is the most important aerosol removal mechanism, the correlation should be negative, which should diminish the AIE. The model can account for the spatial correlation by using different cloud fractions for different aerosol concentration bins (which reduces the forcing by about 15% for CAM5), but it cannot account for the temporal correlation between clouds and aerosol concentration. In addition, it either neglects the influence of the aerosol on cloud liquid water, or it predicts an increase of liquid water with increasing aerosol. Detailed modeling suggests that under some conditions (dry air above an inversion at cloud top), increasing aerosol and droplet number can reduce droplet sedimentation, enhance cloud top entrainment, and decrease cloud liquid water content [*Ackerman et al*., 2004; *Bretherton et al*., 2007; *Guo et al*., 2011]. That mechanism is neglected in this simple model. It also does not explicitly treat the influence of coagulation on the number concentration of primary anthropogenic particles, burying the influence in the difference between the assumed primary particle size and the emitted size.

[81] Compared to other representations of AIEs in IAMs, this simple model provides a stronger physical basis that can be used to quickly explore the parameter space of emissions-climate interactions. The simple model suggests that the dependence of the AIE on aerosol and precursor

emissions may be more linear than the logarithmic representations used in IAMs. AIE estimates by GCMs for different emissions scenarios are needed to improve our fundamental understanding of the AIE and the role of primary emissions in particular, and to confirm this finding. A wide range of forcing values is possible, and parameter values can, in principle, be chosen for consistency with results from detailed global aerosol-climate simulation models.

[82] Fortran code is available from the lead author for application to IAMs or for use as a teaching tool.

[83] **Acknowledgments.** The authors thank colleague Ben Kravitz and reviewers Rob Wood and Chris Golaz for helpful comments. Support for S. Ghan, M. Wang, and K. Zhang was provided by the Office of Science of the U.S. Department of Energy as part of the Atmospheric System Research Program. Support for S. Smith was provided by the U.S. Environmental Protection Agency, Climate Change Division. The Pacific Northwest National Laboratory (PNNL) is operated for the DOE by Battelle Memorial Institute under contract DE-AC06-76RLO 1830.

References

Abdul-Razzak, H., and S. J. Ghan (2000), A parameterization of aerosol activation. Part 2: Multiple aerosol types, *J. Geophys. Res.*, *105*, 6837–6844.

Ackerman, A. S., M. P. Kirkpatrick, D. E. Stevens, and O. B. Toon (2004), The impact of humidity above stratiform clouds on indirect aerosol climate forcing, *Nature*, *432*, 1014–1017, doi:10.1038/nature03174.

Adams, P. J., and J. H. Seinfeld (2003), Disproportionate impact of particulate emissions on global cloud condensation nuclei concentrations, *Geophys. Res. Lett.*, *30*(5), 1239, doi:10.1029/2002GL016303.

Albrecht, B. A. (1989), Aerosols, cloud microphysics, and fractional cloudiness, *Science*, *245*(4923), 1227–1230, doi:10.1126/science.245.4923.1227.

Bauer, S. E., and S. Menon (2012), Aerosol direct, indirect, semidirect, and surface albedo effects from sector contributions based on the IPCC AR5 emissions for preindustrial and present-day conditions, *J. Geophys. Res.*, *117*, D01206, doi:10.1029/2011JD016816.

Bauer, S. E., D. Wright, D. Koch, E. Lewis, R. McGraw, L.-S. Chang, S. Schwarz, and R. Ruedy (2008), Matrix (multiconfiguration aerosol tracker of mixing state): An aerosol microphysical module for global atmospheric models, *Atmos. Chem. Phys.*, *8*, 6003–6035, doi:10.5194/acp-8-6003-2008.

Bennartz, R. (2007), Global assessment of marine boundary layer cloud droplet number concentration from satellite, *J. Geophys. Res.*, *112*, D02201, doi:10.1029/2006JD007547.

Bond, T. C., E. Bhardwaj, R. Dong, R. Jogani, S. Jung, C. Roden, D. G. Streets, and N. M. Trautmann (2007), Historical emissions of black and organic carbon aerosol from energy-related combustion, 1850 – 2000, *Global Biogeochem. Cycles*, *21*, GB2018, doi:10.1029/2006GB002840.

Bretherton, C. S., P. N. Blossey, and J. Uchida (2007), Cloud droplet sedimentation, entrainment efficiency, and subtropical stratocumulus albedo, *Geophys. Res. Lett.*, *34*, L03813, doi:10.1029/2006GL027648.

Chen, Y., and J. E. Penner (2005), Uncertainty analysis for estimates of the first indirect aerosol effect, *Atmos. Chem. Phys.*, *5*, 2935–2948.

Chin, M., R. B. Rood, S.-J. Lin, J.-F. Muller, and A. Thompson (2000), Atmospheric sulfur cycle simulated in the global model GOCART: Model description and global properties, *J. Geophys. Res.*, *105*, 24,671–24,687.

Considine, G., J. A. Curry, and B. Wielicki (1997), Modeling cloud fraction and horizontal variability in marine boundary layer clouds, *J. Geophys. Res.*, *102*, 13,517–13,525.

Denman, K. L., et al. (2007), Couplings between changes in the climate system and biogeochemistry, in *Climate change 2007: The physical science basis*, edited by S. Solomon et al., 129–234 pp., Cambridge University Press, Cambridge, UK.

Donner, L. J., et al. (2011), The dynamical core, physical parameterizations, and basic simulation characteristics of the atmospheric component AM3 of the GFDL global coupled model CM3, *J. Clim.*, *24*, 3484–3519, doi:10.1175/2011JCLI3955.1.

Donohoe, A., and D. S. Battisti (2011), Atmospheric and surface contributions to planetary albedo, *J. Clim.*, *24*, 4402–4418, doi:10.1175/2011JCLI3946.1.

Forster, P., et al. (2007), Changes in atmospheric constituents and in radiative forcing, in *Climate Change 2007: The Physical Science Basis. Contribution of Working Group I to the Fourth Assessment Report of the Intergovernmental Panel on Climate Change*, 129–234, edited by S. Solomon et al., Cambridge Univ. Press, New York.

Ghan, S. J., H. Abdul-Razzak, A. Nenes, Y. Ming, X. Liu, M. Ovchinnikov, B. Shipway, N. Meskhidze, J. Xu, and X. Shi (2011), Droplet nucleation: Physically-based parameterizations and comparative evaluation, *J. Adv. Model. Earth Syst.*, *3*, M10001, doi:10.1029/2011MS000074.

Ghan, S. J., X. Liu, R. C. Easter, R. Zaveri, P. J. Rasch, J.-H. Yoon, and B. Eaton (2012), Toward a minimal representation of aerosols in climate models: Comparative decomposition of aerosol direct, semi-direct and indirect radiative forcing, *J. Climate*, *25*, 6461–6476, doi:10.1175/JCLI-D-11-00650.1.

Golaz, J.-C., M. Salzmann, L. J. Donner, L. W. Horowitz, Y. Ming, and M. Zhao (2011), Sensitivity of the aerosol indirect effect to subgrid variability in the cloud parame- terization of the GFDL Atmosphere General Circulation Model AM3, *J. Climate*, *24*, 3145–3160, doi:10.1175/2010JCLI3945.1.

Golaz, J.-C., L. W. Horowitz, and J. Levy II (2013), Cloud tuning in a coupled climate model: impact on 20th century warming, *Geophys. Res. Lett.*, doi:10.1002/grl.50232, in press.

Guo, H., J.-C. Golaz, and L. J. Donner (2011), Aerosol effects on stratocumulus water paths in a PDF-based parameterization, *Geophys. Res. Lett.*, *38*, L17808, doi:10.1029/2011GL048611.

Haerter, J. O., E. Roeckner, L. Tomassini, and J.-S. von Storch (2009), Parametric uncertainty effects on aerosol radiative forcing, *Geophys. Res. Lett.*, *36*, L15707, doi:10.1029/2009GL039050.

Hallquist, M., et al. (2009), The formation, properties and impact of secondary organic aerosol: current and emerging issues, *Atmos. Chem. Phys.*, *9*, 5155–5236, doi:10.5194/acp-9- 5155-2009.

Hansen, J., M. Sato, and R. Ruedy (1997), Radiative forcing and climate response, *J. Geophys. Res.*, *102*, 6831–6864.

Hill, A. A., G. Feingold, and H. Jiang (2009), The influence of entrainment and mixing assumption on aerosol–cloud interactions in marine stratocumulus, *J. Atmos. Sci.*, *66*, 1450–1464.

Hoose, C., J. E. Kristjánsson, T. Iversen, A. Kirkevåg, Ø. Seland, and A. Gettelman (2009), Constraining cloud droplet number concentration in GCMs suppresses the aerosol indirect effect, *Geophys. Res. Lett.*, *36*, L12807, doi:10.1029/2009GL038568.

Hsieh, W. C., H. Jonsson, L.-P. Wang, G. Buzorius, R. C. Flagan, J. H. Seinfeld, and A. Nenes (2009), On the representation of droplet coalescence and autoconversion: Evaluation using ambient cloud droplet size distributions, *J. Geophys. Res.*, *114*, D07201, doi:10.1029/2008JD010502.

Jathar, S. H., S. C. Farina, A. L. Robinson, and P. J. Adams (2011), The influence of semi-volatile and reactive primary emissions on the abundance and properties of global organic aerosol, *Atmos. Chem. Phys.*, *11*, 7727–7746, doi:10.5194/acp-11-7727-2011.

Kay, J. E. (2012), Exposing global cloud biases in the Community Atmosphere Model (CAM) using satellite observations and their corresponding Instrument simulators, *J. Clim.*, *25*, 5190–5207.

Kaufman, Y. J., and R. S. Fraser (1991), Fossil fuel and biomass burning impact on climate – heating or cooling? *J. Climate*, *4*, 578–588.

Khairoutdinov, M. F., and Y. Kogan (2000), A new cloud physics parameterization in a large-eddy simulation model of marine stratocumulus, *Mon. Wea. Rev.*, *128*, 299–243.

Kiehl, J. T. (2007), Twentieth century climate model response and climate sensitivity, *Geophys. Res. Lett.*, *34*, L22710, doi:10.1029/2007GL031383.

Koch, D., D. Jacob, I. Tegen, D. Rind, and M. Chin (1999), Tropospheric sulfur simulation and sulfate direct radiative forcing in the Goddard Institute for Space Studies general circulation model, *J. Geophys. Res.*, *104*, 23,799–23,822.

Koehler, K. A., S. M. Kreidenweis, P. J. DeMott, M. D. Petters, A. J. Prenni, and C. M. Carrico (2009), Hygroscopicity and cloud droplet activation of mineral dust aerosol, *Geophys. Res. Lett.*, *36*, L08805, doi:10.1029/2009GL037348.

Lacis, A. A., and Hansen, J. E. (1974), Parameterization for the absorption of solar radiation in the earth's atmosphere, *J. Atmos. Sci.*, *31*, 118–133.

Lamarque, J. F., et al. (2010), Historical (1850–2000) gridded anthropogenic and biomass burning emissions of reactive gases and aerosols: methodology and application, *Atmos. Chem. Phys.*, *10*, 7017–7039, doi:10.5194/acp-10-7017-2010.

Lee, L. A., K. S. Carslaw, K. J. Pringle, G. W. Mann, and D. V. Spracklen (2011), Emulation of a complex global aerosol model to quantify sensitivity to uncertain parameters, *Atmos. Chem. Phys.*, *11*, 12,253–12,273, doi:10.5194/acp-11-12253-2011.

Lee, L. A., K. J. Pringle, C. L. Reddington, G. W. Mann, P. Stier, D. V. Spracklen, J. R. Pierce, and K. S. Carslaw (2013), The magnitude and causes of uncertainty in global model simulations of cloud condensation nuclei, *Atmos. Chem. Phys. Discuss.*, *13*, 6295–6378, doi:10.5194/acpd-13-6295-2013.

Liu, Y., P. H. Daum, and R. McGraw (2004), An analytical expression for predicting the critical radius in the autoconversion parameterization, *Geophys. Res. Lett.*, *31*, L06121, doi:10.1029/2003GL019117.

Liu, X., et al. (2012), Toward a minimal representation of aerosol in climate models: Description and evaluation in the Community Atmosphere Model CAM5, *Geosci. Model. Dev.*, *5*, 709–739, doi:10.5194/gmd-5-709-2012.

Lohmann, U., and S. Ferrachat (2010), Impact of parametric uncertainties on the present-day climate and on the anthropogenic aerosol effect, *Atmos. Chem. Phys.*, *10*, 11373–11383, doi:10.5194/acp-10-11373.

Lohmann, U., B. Karcher, and J. Hendricks (2004), Sensitivity studies of cirrus clouds formed by heterogeneous freezing in the ECHAM GCM, *J. Geophys. Res.*, *109*, D16204, doi:10.1029/2003JD004443.

Lohmann, U., P. Stier, C. Hoose, S. Ferrachat, S. Kloster, E. Roeckner, and J. Zhang (2007), Cloud microphysics and aerosol indirect effects in the global climate model ECHAM5-HAM, *Atmos. Chem. Phys.*, *7*, 3425–3446.

Lohmann, U., L. Rotstayn, T. Storelvmo, A. Jones, S. Menon, J. Quaas, A. M. L. Ekman, D. Koch, and R. Ruedy (2010), Total aerosol effect: radiative forcing or radiative flux perturbation?, *Atmos. Chem. Phys.*, *10*, 3235–3246, doi:10.5194/acp-10-3235- 2010.

Manktelow, P. T., G. W. Mann, K. S. Carslaw, D. V. Spracklen, and M. P. Chipperfield (2007), Regional and global trends in sulfate aerosol since the 1980s, *Geophys. Res. Lett.*, *34*, L14803, doi:10.1029/2006GL028668.

Mann, G. W., et al. (2010), Description and evaluation of GLOMAP-mode: a modal global aerosol microphysics model for the UKCA composition-climate model, *Geosci. Mod. Dev.*, *3*, 519–551, doi:10.5194/gmd-3-519-2010.

Martin, G. M., D. W. Johnson, and A. Spice (1994), The measurement and parameterization of effective radius of droplets in warm stratocumulus clouds, *J. Atmos. Sci.*, *51*, 1823–1842.

Meinshausen, M., S. C. B. Raper, and T. M. L. Wigley (2011a), Emulating coupled atmosphere-ocean and carbon cycle models with a simpler model, MAGICC6 – Part 1: Model description and calibration, *Atmos. Chem. Phys.*, *11*, 1417–1456, doi:10.5194/acp-11-1417-2011.

Meinshausen, M., T. M. L. Wigley, and S. C. B. Raper (2011b), Emulating atmosphere-ocean and carbon cycle models with a simpler model, MAGICC6 – Part 2: Applications, *Atmos. Chem. Phys.*, *11*, 1457–1471, doi:10.5194/acp-11-1457-2011.

Menon, S., A. D. Del Genio, D. Koch, and G. Tselioudis (2002), GCM simulations of the aerosol indirect effect: Sensitivity to cloud parameterization and aerosol burden, *J. Atmos. Sci.*, *59*(3), 692–713.

Murphy, D. M., S. Solomon, R. W. Portmann, K. H. Rosenlof, P. M. Forster, and T. Wong (2009), An observationally based energy balance for the Earth since 1950, *J. Geophys. Res.*, *114*, D17107, doi:10.1029/2009JD012105.

Napari, I., M. Noppel, H. Vehkamaki, and M. Kulmala (2002), Parametrization of ternary nucleation rates for H_2SO_4-NH_3-H_2O vapors, *J. Geophys. Res.*, *107*(D19), 4381, doi:10.1029/2002JD002132.

Pan, W., M. A. Tatang, G. McRae, and R. G. Prinn (1998), Uncertainty analysis of indirect radiative forcing by anthropogenic sulfate aerosols, *J. Geophys. Res.*, *103*, 3815–3823.

Penner, J. E., M. Andreae, H. Annegarn, L. Barrie, J. Feichter, D. Hegg, R. L. Jayaraman, D. Murphy, J. Nganga, and G. Pitari (2001), Aerosols, their direct and indirect effects, in *Climate Change 2001: The Scientific Basis, Contribution of Working Group I to the Third Assessment Report of the Intergovernmental Panel on Climate Change*, 289–348, edited by J. T. Houghton et al., Cambridge Univ. Press, New York.

Petters, M. D., and S. M. Kreidenweis (2007), A single parameter representation of hygroscopic growth and cloud condensation nucleus activity, *Atmos. Chem. Phys.*, *7*(8), 1961–1971, doi:10.5194/acp-7-1961-2007.

Petters, M. D., C. M. Carrico, S. M. Kreidenweis, A. J. Prenni, P. J. DeMott, J. L. Collett Jr., and H. Moosmuller (2009), Cloud condensation nucleation activity of biomass burning aerosol, *J. Geophys. Res.*, *114*, D22205, doi:10.1029/2009JD012353.

Pierce, J. R., and P. J. Adams (2009), Uncertainty in global CCN concentrations from uncertain aerosol nucleation and primary emission rates, *Atmos. Chem. Phys.*, *9*, 1339–1356.

Pierce, J. R., K. Chen, and P. J. Adams (2007), Contribution of primary carbonaceous aerosol to cloud condensation nuclei: processes and uncertainties evaluated with a global aerosol microphysics model, *Atmos Chem Phys*, *7*(20), 5447–5466.

Platnick, S., and S. Twomey (1994), Determining the susceptibility of cloud albedo to changes in droplet concentration with the Advanced Very High Resolution Radiometer, *J. Appl. Meteorol.*, *33*, 334–347.

Quaas, J., et al. (2009), Aerosol indirect effects – general circulation model intercomparison and evaluation with satellite data, *Atmos. Chem. Phys.*, *9*, 8697–8717.

Rasch, P. J., and J. E. Kristjansson (1998), A comparison of the CCM3 model climate using diagnosed and predicted condensate parameterization, *J. Climate*, *11*, 1587–1614.

Reddington, C. L., et al. (2011), Primary versus secondary contributions to particle number concentrations in the European boundary layer, *Atmos. Chem. Phys.*, *11*, 12,007–12,036, doi:10.5194/acp-11-12007-2011.

Rosenfeld, D., H. Wang, and P. J. Rasch (2012), The roles of cloud drop effective radius and LWP in determining rain properties in marine stratocumulus, *Geophys. Res. Lett.*, *39*, L13801, doi:10.1029/2012GL052028.

Rossow, W. B., and R. A. Schiffer (1999), Advances in understanding clouds from ISCCP, *Bull. Am. Meteorol. Soc.*, *80*, 2261–2287.

Rotstayn, L. D. (2000), On the "tuning" of autoconversion parameterizations in climate models, *J. Geophys. Res.*, *105*, 15,495–15,507.

Schulz, M., et al. (2006), Radiative forcing by aerosols as derived from the AeroCom present-day and pre-industrial simulations, *Atmos. Chem. Phys.*, *6*, 5225–5246, doi:10.5194/acp-6-5225-2006.

Smith, S. J., J. van Aardenne, Z. Klimont, R. Andres, A. Volke, and S. Delgado Arias (2011), Anthropogenic sulfur dioxide emissions: 1850-2005, *Atmos. Chem. Phys.*, *11*, 1101–1116, doi:10.5194/acp-11-1101-2011.

Spracklen, D. V., et al. (2011), Aerosol mass spectrometer constraint on the global secondary organic aerosol budget, *Atmos. Chem. Phys.*, *11*, 12,109–12,136, doi:10.5194/acp-11-12109-2011.

Stevens, R. G., J. R. Pierce, C. A. Brock, M. K. Reed, J. H. Crawford, J. S. Holloway, T. B. Ryerson, L. G. Huey, and J. B. Nowak (2012), Nucleation and growth of sulfate aerosol in coal-fired power plant plumes: Sensitivity to background aerosol and meteorology, *Atmos. Chem. Phys.*, *12*, 189–206, doi:10.5194/acp-12-189-2012.

Stier, P., et al. (2005), The aerosol climate model ECHAM5-HAM, *Atmos. Chem. Phys.*, *5*, 1125–1156.

Storelvmo, T., J. E. Kristjansson, S. J. Ghan, A. Kirkevag, Ø. Seland, and T. Iversen (2006), Predicting cloud droplet number concentration in Community Atmosphere Model (CAM)-Oslo, *J. Geophys. Res.*, *111*, D24208, doi:10.1029/2005JD006300.

Storelvmo, T., U. Lohmann, and R. Bennartz (2009), What governs the spread in shortwave forcings in the transient IPCC AR4 models?, *Geophys. Res. Lett.*, *36*, L01806, doi:10.1029/2008GL036069.

Takemura, T., T. Nozawa, S. Emori, T. Y. Nakajima, and T. Nakajima (2005), Simulation of climate response to aerosol direct and indirect effects with aerosol transport-radiation model, *J. Geophys. Res.*, *110*, D02202, doi:10.1029/2004JD005029.

Thomson, A. M., et al. (2011), RCP4.5: A pathway for stabilization of radiative forcing by 2100, *Clim. Change*, *109*, 77–94, doi:10.1007/s10584-011-0151-4.

Twomey, S. (1977), Influence of pollution on shortwave albedo of clouds, *J. Atmos. Sci.*, *34*(7), 1149–1152.

Twomey, S. (1991), Aerosols, clouds, and radiation, *Atmos. Environ.*, *25A*, 2435–2442.

Wang, M., and J. E. Penner (2009), Aerosol indirect forcing in a global model with particle nucleation, *Atmos. Chem. Phys.*, *9*, 239–260.

Wang, M., S. Ghan, M. Ovchinnikov, X. Liu, R. Easter, E. Kassianov, Y. Qian, R. Marchand, and H. Morrison (2011), Aerosol indirect effects in a multi-scale aerosol-climate model PNNL-MMF, *Atmos. Chem. Phys.*, *11*, 5431–5455, doi:10.5194/acp-11-5431-2011.

Wang, M., et al. (2012), Strong constraints on cloud lifetime effects of aerosol using satellite observations, *Geophys. Res. Lett.*, *39*, L15709, doi:10.1029/2012GL052204.

Whitby, K. T. (1978), Physical characteristics of sulfur aerosols, *Atmos. Environ.*, *12*(1–3), 135–159, doi:10.1016/ 0004-6981(78)90196-8.

Wigley, T. M. L., and S. C. B. Raper (1992), Implications for climate and sea level of revised IPCC emissions scenarios, *Nature*, *357*, 293–300.

Wood, R., and J. P. Taylor (2001), Liquid water path variability in unbroken marine stratocumulus clouds, *Q. J. Roy. Meteorol. Soc.*, *127*, 2635–2662.

Wood, R., T. L. Kubar, and D. L. Hartmann (2009), Understanding the importance of microphysics and macrophysics for warm rain in marine low clouds. Part II: Heuristic models of rain formation, *J. Atmos. Sci.*, *66*, 2974–2990.

Zhang, K., et al. (2012), The global aerosol-climate model ECHAM-HAM, version 2: Sensitivity to improvements in process representations, *Atmos. Chem. Phys.*, *12*, 8911–8949, doi:10.5194/acp-12-8911-2012.